

# Implementing a GPU-based parallel MAX-MIN Ant System

Rafał Skinderowicz<sup>a</sup>

<sup>a</sup>University of Silesia in Katowice, Faculty of Science and Technology,  
Będzińska 39, 41-205 Sosnowiec, Poland

©2020. This manuscript version is made available under the CC-BY-NC-ND 4.0 license  
<http://creativecommons.org/licenses/by-nc-nd/4.0/>

---

## Abstract

The MAX-MIN Ant System (MMAS) is one of the best-known Ant Colony Optimization (ACO) algorithms proven to be efficient at finding satisfactory solutions to many difficult combinatorial optimization problems. The slow-down in Moore's law, and the availability of graphics processing units (GPUs) capable of conducting general-purpose computations at high speed, has sparked considerable research efforts into the development of GPU-based ACO implementations. In this paper, we discuss a range of novel ideas for improving the GPU-based parallel MMAS implementation, allowing it to better utilize the computing power offered by two subsequent Nvidia GPU architectures. Specifically, based on the weighted reservoir sampling algorithm we propose a novel parallel implementation of the node selection procedure, which is at the heart of the MMAS and other ACO algorithms. We also present a memory-efficient implementation of another key-component – the tabu list structure – which is used in the ACO's solution construction stage. The proposed implementations, combined with the existing approaches, lead to a total of six MMAS variants, which are evaluated on a set of Traveling Salesman Problem (TSP) instances ranging from 198 to 3,795 cities. The results show that our MMAS implementation is competitive with state-of-the-art GPU-based and multi-core CPU-based parallel ACO implementations: in fact, the times obtained for the Nvidia V100 Volta GPU were up to 7.18x and 21.79x smaller, respectively. The fastest of the proposed MMAS variants is able to generate over 1 million candidate solutions per second when solving a 1,002-city instance. Moreover, we show that, combined with the 2-opt local search heuristic, the proposed parallel MMAS finds high-quality solutions for the TSP instances with up to 18,512 nodes.

*Keywords:* parallel MAX-MIN Ant System, weighted reservoir sampling, Ant Colony Optimization, GPU, CUDA

---

## 1. Introduction

Ant Colony Optimization (ACO) is a population-based metaheuristic inspired by the social behavior of ants [15]. It has been successfully applied in solving many NP-hard problems, including the Traveling Salesman Problem (TSP), the Quadratic Assignment Problem, and the Sequential Ordering Problem [40, 43, 44]. Being metaheuristic, the ACO does not guarantee finding an optimum solution, however it is often able to offer satisfactory *approximate* solutions within an acceptable time compared to exact methods [28]. However, even metaheuristics can be prohibitively time consuming if faced with a large enough problem instance. For this reason, a lot of research attention has been devoted both to improving the effectiveness of the ACO search process, and to speeding up its execution [33]. The idea of applying GPU-based computing to the ACO is an example of the latter. In recent years, the use of graphics processing units (GPUs) to speed up scientific computations has become commonplace. This has been, in part, dictated by the slow-down in Moore's law, and the progress made in the GPU architecture development, which has resulted in more computing capacity, flexibility, and ease-of-use [46]. In fact, currently a significant proportion of the world's fastest supercomputers is equipped with GPUs to accelerate their computations [42]. Still, the efficient use of the computing capacity offered by GPUs remains a difficult task [23].

---

*Email address:* rafal.skinderowicz@us.edu.pl (Rafał Skinderowicz)

In an ACO, a population of agents (ants) construct, in parallel, a set of solutions to the optimization problem being tackled. Unfortunately, the inherent parallel nature of the ACO does not translate easily into an efficient GPU-based parallel implementation [7, 12, 39]. The difficulties arise partly from the fact that not all of the ACO computations are independent, e.g., pheromone trail updates; as well as from the computing restrictions inflicted by GPU architectures. Although considerable research attention has been devoted to using GPUs to speed up the ACO-based algorithms, both the improved computational capabilities of successive generations of GPUs as well as novel algorithmic ideas, offer new opportunities for greater progress.

In this paper, we present a GPU-based parallel implementation of the MAX-MIN Ant System (MMAS), which is one of the best-performing ACO variants for solving various optimization problems including the production-distribution scheduling problem [22], the blocks relocation problem [24], the routing and scheduling of home health care caregivers problem [13], and the traveling purchaser problem [41]. Building on existing research we show how each of the essential MMAS components can be parallelized to allow the efficient use of the significant computing power offered by the current generation of GPUs.

The main contributions presented in this paper can be summarized as follows:

- We present a novel parallel implementation of the next node (proportional) selection procedure used in the MMAS and other ACO algorithms. The implementation is based on the weighted reservoir sampling algorithm and fits well within the parallel computing model of contemporary GPU architectures.
- We present a novel, memory-efficient implementation of the tabu list structure used by the ACO solution construction process. The implementation allows for the better utilization of fast, but very size limited, shared memory of GPUs.
- Combining these novel ideas and the solutions from the literature, we present a total of six MMAS variants and evaluate their computational efficiency based on two subsequent generations of Nvidia GPUs, namely Pascal and Volta.
- The computational evaluation based on a set of TSP instances ranging from 198 to 3,795 cities shows that the proposed GPU-based MMAS is competitive with state-of-the-art GPU-based [11, 12, 8] and multi-core CPU-based [53] parallel ACO implementations. The times obtained were up to 7.18x and 21.79x smaller, respectively.
- Acknowledging, that the ACO algorithms are typically paired with an efficient, problem-specific local search (LS) method, we combine the proposed GPU-based MMAS with a parallelized 2-opt heuristic. The computational experiments that consider the TSP instances of up to 18,512 nodes show that the proposed implementation is able to generate high-quality solutions, i.e., within 1% from an optimum, in a relatively short time.

The remainder of this paper is organized as follows. In Section 2 we provide a brief description of the MAX-MIN Ant System and short piece on the characteristics of general-purpose GPU computations. Section 3 summarizes the existing work on applying GPUs in speeding up ACO computations, including the MMAS. Our main ideas on the efficient implementation of the GPU-based MMAS are presented in Section 4; while Section 5 presents an analysis of the computational experiments we conducted in order to evaluate the proposals, and compare them with the work described in the literature. Finally, we summarize our findings and provide a few ideas for future work in Section 6.

## 2. Background

### 2.1. MAX-MIN Ant System

The ACO metaheuristic belongs to a group of swarm-based metaheuristics (SBMs) in which the problem-solving abilities are a result of the interactions of simple information-processing units (agents) [25]. The inspirations for the SBMs often come from biological systems including ant colonies, swarms of bees, flocks of birds, and schools of fish, among others [18]. Typically, the agents in the SBMs follow simple rules and are given a certain degree of autonomy, e.g., in selecting the next action to perform. The agents may also interact with each other, e.g., by transferring data about the solutions found, or with the environment, e.g.,

by depositing artificial pheromone trails that can be read by other agents (indirect communication). In addition to ACO, one of the most-successful SBMs are particle swarm optimization (PSO) and artificial bee colony algorithms.

In the MMAS, a number of ants (agents) iteratively construct solutions to a combinatorial optimization problem (COP) [43]. In this paper, we focus on the TSP, following the existing research on parallel ACO [3, 11, 12, 14, 51, 8], although, in principle, the ACO algorithms can be applied to any COP [15].

The TSP can be defined using a complete graph  $G = (V, A)$ , where  $V$  is a set of nodes numbered from 0 to  $n - 1$  ( $n$  being the number of cities), and  $A$  as the set of edges (arcs) between the nodes, i.e.,  $E = \{(i, j) : i, j \in V, i \neq j\}$ . The set of nodes represents a set of cities to be visited by a salesman, while each edge in  $E$  corresponds to a road between a pair of cities. Additionally, for every edge,  $(i, j)$ , a positive value,  $d_{ij}$ , is given, which represents the distance (weight) between the cities,  $i$  and  $j$ . If the TSP is *symmetric*, then  $d_{ij} = d_{ji}$ , otherwise the instance is asymmetric (ATSP) and the distance from  $i$  to  $j$  might not equal the distance from  $j$  to  $i$ . Typically, the distances between the nodes in graph  $G$  satisfy the triangle inequality but, in general, they may be arbitrary. Solving the TSP is equivalent to finding the minimum weight Hamiltonian cycle in graph  $G$ . In general, solving the Hamiltonian cycle is an NP-hard problem and finding the optimum to the TSP is at least as difficult. A comprehensive overview of both exact and approximate approaches to solving the TSP can be found in the work of Applegate et al. [2].

In the ACO, the edges of graph  $G$  correspond to the *solution components* from which the ants' solutions are being constructed. Additionally, for every edge,  $(i, j) \in E$ , there is an associated *pheromone trail*,  $\tau_{ij}(t)$ , where  $t$  denotes a (discrete) time. In nature, the pheromones are chemical substances that some ant species use as an indirect medium of communication between individuals [15]. In ACOs, including the MMAS, the artificial pheromone trails are stored as positive real values, and influence the probability of including the corresponding solution components into the solutions being constructed by the ants. In the MMAS, in contrast to other ACO algorithms, the values of the pheromone trails are *bounded* by limits:  $\tau_{\min}$  and  $\tau_{\max}$  [43].

In the MMAS, an ant starts its solution construction process from an initial node and in each of the subsequent steps it selects an edge (a solution component) that connect its current node with one of the neighboring, as yet unvisited, nodes. The choice of an edge is probabilistic and depends on so-called *heuristic information* (available *a priori*) and the values of the pheromone trails. Specifically, an ant,  $k$ , positioned at node  $i$  selects an edge,  $(i, j)$ , leading to node  $j$  with the probability:

$$p_{ij}^k(t) = \frac{[\tau_{ij}(t)]^\alpha [\eta_{ij}]^\beta}{\sum_{l \in \mathcal{N}_i^k} [\tau_{il}(t)]^\alpha [\eta_{il}]^\beta} \quad \text{if } j \in \mathcal{N}_i^k, \quad (1)$$

where  $\tau_{ij}(t)$  is the value of the pheromone trail deposited on the edge,  $(i, j)$ ;  $\eta_{ij}$  is the value of the heuristic information for the edge,  $(i, j)$ ;  $\alpha$  and  $\beta$  are parameters that control the relative influence of the pheromone values and the heuristic information on the probability; and, finally,  $\mathcal{N}_i^k$ , denotes the set of nodes that neighbor  $i$  to be visited the ant,  $k$ . The heuristic information,  $\eta_{ij}$ , specifies how *attractive* a particular edge  $(i, j)$  is, and in the case of the TSP,  $\eta_{ij} = 1/d_{ij}$ , makes an edge more attractive the shorter it is. This is based on the assumption that good quality solutions consist of edges connecting nodes located near to each other [19]. Each ant stores the previously visited cities in a *tabu list*, which allows  $\mathcal{N}_i^k$  to be computed, guaranteeing that only valid Hamiltonian cycles are constructed.

The pseudocode for the MMAS is shown in Fig. 1. At first, the initial pheromone trail limits,  $\tau_{\min}$  and  $\tau_{\max}$ , are computed based on a solution constructed using the nearest neighbor heuristic. Next, the pheromone trails values are set to  $\tau_{\max}$  (line 2). In the main loop of the algorithm (lines 4–18), each ant constructs a complete solution to the problem starting from a randomly chosen node. After the solutions have been constructed, the *iteration best* solution is selected (line 13). If it is shorter than the current *global best* solution, it becomes the new global best, and the trail limits are updated accordingly. Finally, a pheromone update is performed. This means lowering (evaporating) the values of the pheromone trails:  $\tau_{ij} \leftarrow \max(\rho\tau_{ij}, \tau_{\min})$ , where  $\rho$  is a parameter that controls the evaporation speed. The values of the pheromone trails never drop below the minimum value,  $\tau_{\min}$ , which ensures that all edges have a non-zero probability of being selected even in the late stages of the algorithm's execution. The pheromone trails' values only increase if they correspond to the components of the current iteration's best solution (line 18).

```

1 Calculate pheromone trails limits:  $\tau_{\min}$  and  $\tau_{\max}$ 
2 Set pheromone trails values to  $\tau_{\max}$ 
3  $global\_best \leftarrow \emptyset$ 
4 for  $i \leftarrow 1$  to  $\#iterations$  do
5   for  $j \leftarrow 0$  to  $\#ants - 1$  do
6      $u \leftarrow \mathcal{U}\{0, n - 1\}$  // Select the first node randomly
7      $route_{Ant(j)}[0] \leftarrow u$ 
8     Add  $u$  to  $tabu_{Ant(j)}$ 
9     for  $k \leftarrow 1$  to  $n - 1$  do // Complete the solution (route)
10       $u \leftarrow \text{select\_next\_node}(route_{Ant(j)}[k - 1], tabu_{Ant(j)})$ 
11       $route_{Ant(j)}[k] \leftarrow u$ 
12      Add  $u$  to  $tabu_{Ant(j)}$ 
13    $iter\_best \leftarrow \text{select\_shortest}(route_{Ant(0)}, \dots, route_{Ant(\#ants-1)})$ 
14   if  $global\_best = \emptyset$  or  $iter\_best$  is shorter than  $global\_best$  then
15      $global\_best \leftarrow iter\_best$ 
16     Update pheromone trails limits  $\tau_{\min}$  and  $\tau_{\max}$  using  $global\_best$ 
17   Evaporate pheromone according to  $\rho$  parameter
18   Deposit pheromone based on  $iter\_best$ 

```

Figure 1: The MAX-MIN Ant System.

The values are increased according to:  $\tau_{ij} \leftarrow \min(\tau_{ij} + \Delta_{ij}, \tau_{\max})$ , where

$$\Delta_{ij} = \begin{cases} \text{cost}(iter\_best)^{-1}, & \text{if } (i, j) \in iter\_best, \\ 0, & \text{otherwise.} \end{cases}$$

Increasing pheromone levels for the trails corresponding to the edges (solution components) of good quality solutions, increases the probability that, in subsequent iterations, the ants will choose these edges more often. This process allows the algorithm to learn and construct higher quality solutions over time [15].

It is possible to use the current *global best* value instead of the iteration best [43]. It is worth noting, that in contrast to the Ant Colony System (ACS), parallelization is made simpler because the MMAS *lacks* a local pheromone update [39]. In fact, the pheromone trail values remain constant during the solution construction phase, allowing a *beforehand* computation of the product of the pheromone trails and the heuristic values required by Eq. (1). This optimization is in common use as it reduces both the computation time, and more importantly, the number of loads from the memory [7, 12]. We also apply it in our work, storing the product in a matrix called *choice\_info*.

A single iteration of the MMAS has a  $O(mn^2)$  time complexity, as each of the  $m$  ants constructs a complete solution to the problem in  $n - 1$  steps (assuming that the starting node is chosen arbitrarily),  $n$  being the size of the problem instance. Each step has a complexity of  $O(n)$  as an ant has to move from the current node to the next, chosen from up to  $n - 1$  unvisited nodes. If candidate lists are used, the average complexity of the solution construction process falls to  $O(n \cdot cl) = O(n)$ , where  $cl$  is a constant that denotes the size of the list.

## 2.2. General-purpose computing using GPUs

Architectural differences between the CPUs and the GPUs allow the latter to offer a higher computing power but often at the cost of reorganizing the structure of the calculations to enable parallel execution [26]. For the sake of clarity of further discussion, it is worth clarifying the distinction between *parallelism* and *concurrency*. Assuming that the required computations were divided into independent portions or tasks, parallel execution refers to the case in which the available processing elements (cores) execute the tasks *at the same time*. Concurrency, on the other hand, is a more general term also including the cases in which some of the computations may not overlap in time. In the simplest case, concurrent computations require only a single computing unit working in a time-shared manner. In other words, concurrency allows to handle

multiple computing tasks *at once*, while parallelism emphasises doing multiple computations *at the same time*.

GPUs allow for a high degree of parallelism as they typically contain several replicated *streaming multiprocessors* (SMs), each comprising a number of *processing elements* that share control units, a register file, caches, and shared memory. However, the number of computational tasks should typically exceed the number of available processing elements. This is helpful in situations in which the computations get stalled, e.g., while waiting for the data to be read from memory. In such cases, it is possible to switch to another task for which the necessary data are available. Somewhat related is the description of GPUs as being *throughput-oriented* meaning that a large number of computations can be performed in a given period of time, however, the speed of execution of individual computations could be low compared with that of CPUs [26].

SMs schedule and execute hundreds of parallel threads in groups of 32 called *warps*. The warps employ a model called a *single-instruction, multiple-thread* (SIMT), in which all threads start at the same program address and typically execute the same instructions over different data (data-parallelism). However, each thread has its own program counter and register state so its execution may diverge from the other threads in the warp. From the performance point of view, it is best to keep the number of diverging executions as low as possible; although, in the newer Nvidia architectures (Volta, Turing) the penalty paid is lower than previous versions [23]. It is also worth adding that the threads within a warp have access to primitives allowing them to access each other's registers directly, i.e., without the need for accessing slower, shared memory.

Nvidia's Compute Unified Device Architecture (CUDA) provides a *programming model* that forms an abstract layer over the hardware architecture [1]. The CUDA divides programs into CPU (host) and GPU (device) parts. The host and the device have separate memory spaces, but a unified memory extension exists in CUDA 6.0 (and newer versions) that allows the CPU and GPU threads to store data in a shared address space. A programmer can define functions, called *kernels*, which are executed by the GPU. Each kernel is executed by a specified number of concurrent threads that are divided into several *blocks*, which in turn are organized into a *grid*. Each thread-block is assigned to a single SM and can communicate through the shared memory with the other threads within the same block. The blocks are scheduled independently; hence, threads belonging to separate blocks can only communicate using large but high-latency global memory.

Summarizing, each thread executing on the GPU has access to a memory hierarchy, with the privately-accessed registers being the fastest, the shared memory being a bit slower, a small but cached *constant memory* also offering relatively fast reads, and, finally, the global memory being the slowest. L1 and L2 caches are also present but not directly accessible to the programmer. The CUDA programming model assumes that a large number of threads (tens of thousands) is executed concurrently to allow memory-related latencies to be hidden.

### 3. Related work

Being a population-based metaheuristic, the ACO naturally exhibits some degree of parallelism [15]. For example, there is no direct communication between the ants. In fact, the ants cooperate *indirectly* (stigmergy) by modifying the values of the pheromone trails that correspond to the components of the problem they select during the solution construction phase. If the solutions are constructed quickly, as they are in the case of the TSP, the frequent updates of the pheromone trails become problematic from the parallelization point of view. Overall, a lot of research has been devoted to the parallelization of the ACO, especially for execution on multi-CPU systems aimed at both improving the quality of the generated solutions, and shortening the execution time [34, 10, 30]. A good summary of the research was done by Pedemonte et al. [33]. Although valuable, the CPU-based parallelization of the ACO is difficult to transfer directly to the GPUs due to differences in the hardware architectures. In most of the approaches to CPU-based ACO parallelization, a coarse-grained organization of computations is favored, with the multi-colony ACO being one of the most efficient. The GPUs on the other hand, are *throughput oriented* and contain thousands of relatively simple processing elements. Only recently has the increasing number of CPU cores and the availability of wide vector instructions (e.g. AVX2) allowed for a more efficient, fine-grained approach [51]. For these reasons, the rest of the section will focus on research that targets the GPU-based parallelization of the ACO.

The first attempts at using GPUs to speedup the ACO predate the CUDA programming framework. Catala et al. [6] presented a parallel ACO for solving the Orienteering Problem, although some speed increases were reported, the implementation was complicated as the authors had to use graphics generation primitives

to perform computations. A similar programming approach was used by Wang et al. [50], who proposed a GPU-based MMAS. The authors reported a modest speedup compared to a sequential, CPU-based MMAS implementation.

### 3.1. Task-based vs data-parallel approaches

One of the first attempts to speed up the MMAS using the first generation of general purpose GPUs was made by Bai et al. [3]. This approach used multiple ant colonies with a single colony assigned to a single thread block, and each thread within the block assigned to an ant. The distance matrix was stored in texture memory to facilitate cache memory. Computational experiments showed the execution was around 2x faster than a reference CPU implementation when solving the TSP. This is an example of *task-based* parallelism, as the threads are directly mapped to the ants. The problem with this approach is that it leads to *warp-branching*, i.e., different threads within a thread-warp (using the Nvidia CUDA-based terminology) are likely to take different execution paths as the ants follow divergent paths, causing the remaining threads to wait.

A more efficient, *data-parallel* approach was proposed by Cecilia et al. [7]. In that implementation, a single thread block is mapped to a single ant in the Ant System (AS), that is, all threads within a thread block work on a single solution to the problem. This avoids the warp-branching present in the task-based approach as the threads execute the same instructions but for different data, i.e., nodes. The authors considered block sizes of 16 to 1,024 threads. The computational experiments done on the Nvidia Tesla C2050 GPU showed that the best performance was obtained for 128 threads per block. The work’s most notable contribution was the introduction of the so-called *I-Roulette* (independent roulette) method for selecting, in parallel, the next city to be visited by an ant. This was the alternative to the proportional selection method, also known as the Roulette Wheel Method (RWM), which was used originally. In the I-Roulette method, the probabilities of selecting each of the unvisited nodes (assigned to separate threads) are multiplied by random numbers, and the node that has the maximum product is selected through a parallel reduction. Although, the I-Roulette method did not produce the same results as the sequential RWM, it was up to 2.36x faster. The authors also considered two parallel pheromone update methods, in which the simpler one used atomic instructions to allow the safe simultaneous modification of memory by multiple threads. Overall, the reported speedups were up to 20x faster compared to the sequential implementation.

A valuable comparison between the task-based and data-parallel approaches can be found in the work of Delévacq et al. [14] who presented a GPU-based parallel implementation of the MMAS for the TSP. In the task based approach, each ant was assigned to a CUDA thread. In the data-parallel approach, a whole thread-block was assigned to a single ant. Moreover, the 3-opt local search for improving the ants’ solutions was also included in both approaches. The data-parallel approach was significantly faster than the task-based one, and up to 19.47x faster than the reference sequential implementation. The inclusion of the 3-opt resulted in more modest speedups of up to 8.03x for the data-parallel implementation. The authors concluded that the 3-opt is not well suited to GPU architecture as it has a low computation to memory access (reads and writes) ratio.

### 3.2. Alternative Implementations of the RWM

The I-Roulette method used by Cecilia et al. [7] was analyzed, both experimentally and analytically, by Lloyd and Amos [27] who concluded that it behaves in a *qualitatively* different way to the RWM. Specifically, it tends to increase the probability of selecting an edge with a high pheromone value in cases where there are a large number of edges to choose from and the majority of the pheromone is concentrated on one edge. This results in a slight degradation in the quality of MMAS solutions for TSP instances with more than 1,000 nodes. On the other hand, there is also a slight improvement in the quality of the solutions produced by the parallel ACS.

Another approach to speeding up the AS on GPUs was proposed by Uchida et al. [47]. In this algorithm, the RWM was replaced by a method called the *stochastic trial*. The stochastic trial utilizes a matrix that has its rows assigned to the nodes, each containing the prefix sums of the selection probabilities for the corresponding node. During the solution construction phase, an ant located at the node,  $i$ , draws a uniform number from the range  $[0, 1]$  and checks if the cell from the  $i$ -th row of the matrix corresponds to an unvisited node. If it does, it is selected, otherwise the process is repeated a specified number of times. In the case of a

failure, the next node is selected using a (slower) parallel RWM. Together with a parallel pheromone update method, the proposed algorithm was up to 43.47x faster than a sequential AS executed on a CPU.

The data-parallel approach was also adopted by Dawson and Stewart [12] who applied a GPU-based AS to the TSP. The authors proposed a new, efficient parallel implementation of the RWM – the Double-Spin Roulette (DS-Roulette) method. The DS-Roulette method consists of three stages. In the first stage, all nodes are divided between four thread warps (128 threads). Within a warp, the yet to be visited nodes (cities) are determined, and the threads perform a warp-level reduction of the selection probabilities that correspond to the nodes. In the second stage, the reduced values are used by the RWM to select a winning warp. In the third stage, the winning warp draws a second random number and performs a node selection from the assigned nodes. The selected node becomes the final result of the DS-Roulette execution. The DS-Roulette method avoids the block-level reduction, and its results are closer to the results of the sequential RWM when compared to the proposals of Uchida et al. [47] and Cecilia et al. [7]. Combined with a parallel pheromone update, the resulting algorithm was up to 82.3x faster than the CPU-based implementation when tested on the Nvidia GTX 580 GPU.

In subsequent work, Dawson and Stewart [11] presented a parallel AS in which candidate lists were used to speed up the node selection process. By limiting the length of the candidate list to 32 they were able to exploit the warp-level communication primitives provided by the CUDA to efficiently implement the RWM. Along with the tabu list compression method by Uchida et al. [47], the resulting implementation was up to 18x faster than its sequential counterpart.

### 3.3. Recent Advancements

In recent work, Cecilia et al. [8] discussed several aspects of an efficient GPU-based AS implementation. Specifically, they introduced a parallel implementation of the RWM that uses scan and stencil patterns to efficiently select an unvisited node. To further speed up the calculations, the authors applied a partial synchronization between the warps within thread-blocks to create a *super-warp* comprised of two warps (64 threads). Combined with the previous parallel pheromone update methods [7], the resulting implementation, being *state-of-the-art*, was up to 8x faster than the baseline version proposed earlier.

The most recent proposals include work by Borisenko and Gorlatch [5] who presented a GPU-based parallel implementation of the ACO, combined with Simulated Annealing (SA) for the optimization of the multi-product batch plants used, e.g., in the chemical industry. The proposed metaheuristic was able to quickly find near-optimal solutions, making it a viable alternative to the exact, but very time-consuming, branch-and-bound approach. Another work, by Rey et al. [36], discusses an interesting hybrid-parallel ACO for solving the Vehicle Routing Problem (VRP). The first stage of the algorithm consists of the MMAS being executed on the GPU and generating TSP routes which are then combined into the VRP solutions and improved using LS procedures during the second stage being executed on the CPU. The GPU-based MMAS is also one of components in the recently proposed parallel framework for the Multi-population Cultural Algorithm by Unold and Tarnawski [48].

One should also be aware that a lot of work has been done on efficient parallel implementations of other SBMs including the PSO [31] and bees algorithm [29]. A more general summary can be found in the work of Tan and Ding [45].

## 4. Implementing a GPU-based MMAS

In this section we discuss how the MMAS can be parallelized in order to achieve efficient execution on GPUs. We devote most of our attention to the solution construction phase of the algorithm which is its most time-consuming part.

### 4.1. Tabu implementation

In order to calculate the probabilities defined by Eq. (1) it is necessary to determine the set of nodes yet to be visited by an ant. In the Ant System, the MMAS, and other ACO algorithms, the nodes already visited by the ant are typically stored in a data structure called a *tabu list* [16]. If the nodes are added in the order in which they are visited by the ant, then the tabu list comprises a partial solution to the problem, which, at the end of the construction phase, becomes the complete solution. It is worth noting, that in order to

calculate the probabilities given by Eq. (1) it is necessary to determine the, as yet, unvisited nodes, however, the relative order in which they are considered is not important. In fact, we want the tabu list to fit into the fast but small shared memory of the GPUs’ SMs. Hence, we can generalize the notion of the tabu list (or *tabu* for short – to avoid confusion) to any data structure that provides the following operations:

- `mark( $v$ )` – marks node  $v$  as *visited*;
- `is_visited( $v$ )` – returns `true` if the node  $v$  has already been visited by an ant, or otherwise `false`;
- `length()` – returns a number that is equal to or *greater* than the number of yet unvisited nodes;
- `get_candidate( $i$ )` – where  $i \in \{0, 1, \dots, \text{length}() - 1\}$ , returns either an unvisited node  $u$ ,  $u \in V$ , or a special *sentinel* value  $s$ ,  $s \notin V$ ; we assume that if `get_candidate()` is executed for every  $i \in \{0, 1, \dots, \text{length}() - 1\}$  then the returned set of values contains all the nodes to be visited by an ant.

The non-obvious definition of `get_candidate()` allows the tabu list to be implemented using a *bitmask*. The general scheme for accessing the set of nodes to be visited using the presented operations is shown in Fig. 2.

```

1 l ← tabu.length();
2 for i ← 0 to l - 1 do
3   v ← tabu.get_candidate(i);
4   if v ≠ sentinel then
5     v can be processed;
```

Figure 2: General scheme for processing the tabu using the generalized scheme (see Sec. 4.1)

It is worth emphasising that the tabu is at the core of the MMAS and other ACO algorithms, and its implementation is important for the efficiency of the whole algorithm. In case of GPUs, the tabu should be stored in the *shared* (local) memory so that it can be accessed quickly [7]. Unfortunately, the size of the shared memory available to each thread block is very limited – usually only 48kB to 96kB in the last few generations of Nvidia GPUs [23]. Hence, both the time and space complexity of the tabu are important.

A simple linked list is sufficient to implement all of the tabu operations, however accessing an arbitrary element in the list has  $O(n)$  time complexity, with  $n$  being the number of nodes. A more efficient implementation, known as the *tabu with list compression* (LC), has been described by Dawson and Stewart [11], who applied the *list compression method* first proposed by Uchida et al. [47]. The data structure consists of two single dimensional arrays of integers of size  $n$ , and a variable  $L$ . For the sake of simplicity, let’s denote them by *unvisited* and *indices*. The first one, stores the list of  $L$  nodes to be visited by an ant, while the second stores the indices of every node in the first list. For example, if  $unvisited[i] = v$  then  $indices[v] = i$  (we assume that the nodes are denoted by numbers from 0 to  $n - 1$ ). At the start of the construction process, both arrays contain a sequence of  $n$  consecutive integers from 0 to  $n - 1$ , where  $n$  is the number of nodes and  $L = n$ . In subsequent steps, if a node,  $v = unvisited[i]$ , is being visited, then the `mark( $v$ )` operation involves the updates:  $unvisited[i] \leftarrow unvisited[L - 1]$ , i.e., the visited node is replaced by the last one, and  $indices[unvisited[i]] \leftarrow i$ , is followed by  $L \leftarrow L - 1$ . It can be seen that, if  $indices[u] \geq L$  then the node,  $u$ , has already been visited by the ant. Figure 3 shows an example of how the LC works.

The LC allows all the tabu operations to be performed in constant time. The major disadvantage is the necessity for storing two  $n$ -element arrays in the memory. On the other hand, the *indices* array allows the order in which the nodes were visited (in reverse order) to be recovered. For example, if we consider the case shown in Fig 3, nodes 2, 5 and 7 were already visited, and the corresponding values in the *indices* array are equal to 7, 6 and 5. By subtracting each value from  $n - 1$  we get  $n - 1 - 7 = 0$ ,  $n - 1 - 6 = 1$  and  $n - 1 - 5 = 2$ , respectively, which is exactly the order in which the nodes were visited.

By analyzing the LC tabu, we notice that it is possible to implement the tabu using only one list, *entries*, of length  $n$ , and a variable,  $L$ . The trick is to divide the *entries* (logically) into two parts. The first (left) part consists of the first  $L$  ( $L \leq n$ ) entries and contains the list of  $L$  distinct nodes to be visited, i.e.,  $entries[i] = u$ ,  $i < L$  if, and only if, node  $u$  is as yet unvisited. The second (right) part comprises entries at positions from  $L$  up to  $n - 1$ . It is used to store indices for the nodes *yet to be visited* that were relocated to



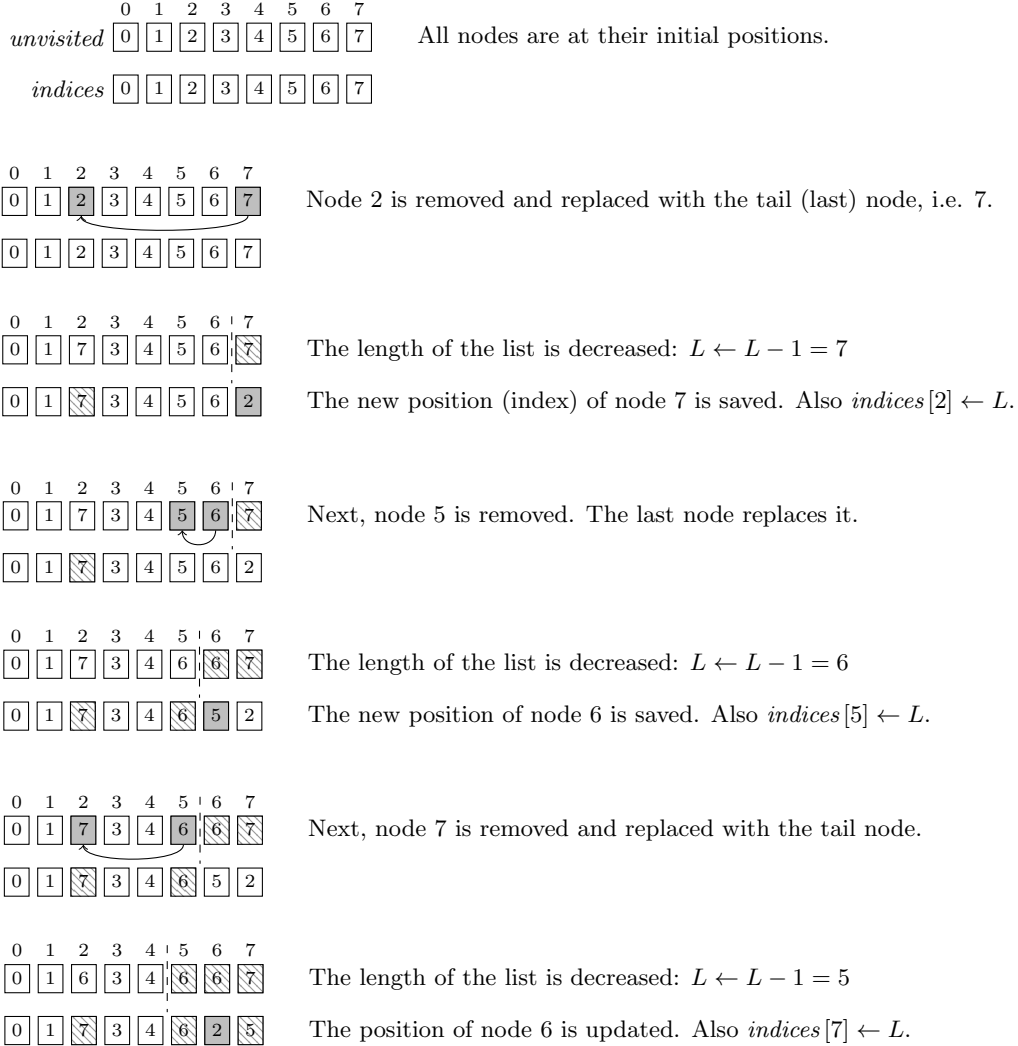


Figure 3: An example showing the subsequent removal of nodes 2, 5, and 7 from the LC tabu, which contains nodes 0 to 7. The dashed line marks the end of the nodes list.

the left part, or the *sentinel* value of  $n$  for the nodes that have already been *visited*, i.e., are not in the left part.

Initially, the *entries* array contains consecutive numbers from 0 to  $n - 1$ , denoting the unvisited nodes. In subsequent steps, if a node,  $u$ , is visited, one of two cases is possible: either  $u < L$  or  $u \geq L$ . In the first case, the node  $u$  is at its initial position, i.e.,  $entries[u] = u$ . In the second case, the node has been relocated to the left part, and the value  $i_u = entries[u]$  denotes the *index* at which the node is currently located, i.e.,  $entries[i_u] = u$ . If  $i_u = L - 1$  then  $u$  is at the end of the list, and it is enough to set  $entries[i_u] \leftarrow n$  to mark that node  $u$  has been visited. Otherwise,  $i_u < L - 1$  and the last element,  $t = entries[L - 1]$ , of the list replaces it:  $entries[i_u] \leftarrow t$ . The new position of  $t$  is saved:  $entries[t] \leftarrow i_u$ . It is worth noting that this scheme allows for checking in  $O(1)$  time whether node  $u$  was visited, simply by checking whether  $entries[u] > u$ . We will refer to this tabu implementation as the *compact tabu* (CT). An example showing the removal of three nodes from a CT that contains eight nodes is shown in Fig. 4.

Even more memory efficient implementation can be achieved if a *bitmask* of length  $n$  is used to mark the visited /unvisited state of each node. In that case, the `mark` and `is_visited` tabu operations can be performed in  $O(1)$  time. However, accessing the unvisited nodes (Fig. 2) requires checking the state of  $n$  bits, while the two previous tabu implementations provide *direct* accesses to the *unvisited* nodes. For the sake of completeness, we will refer to this tabu as the *bitmask tabu* (BT). A summary of the presented tabu

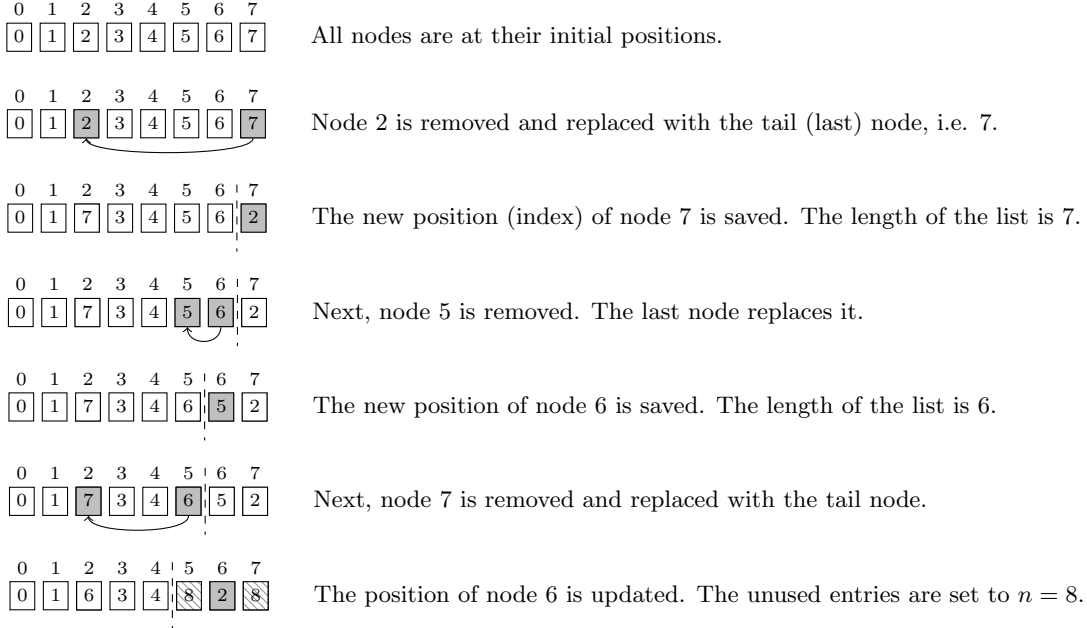


Figure 4: An example showing the subsequent removal of nodes 2, 5, and 7 from a CT containing nodes 0 to 7. The dashed line marks the end of the nodes list. The entries to the right of the dashed line are used to store positions (indices) for the nodes relocated to the left.

Table 1: A summary of the considered tabu implementations. We assume that the nodes are denoted as numbers 0 to  $n - 1$ , where  $n < 2^{16}$ , i.e. a node can fit into an unsigned 16-bit variable.

Tabu characteristic	Tabu implementation		
	TLC	CT	BT
Testing if node was visited ( <code>is_visited</code> )	$O(1)$	$O(1)$	$O(1)$
Marking node as visited ( <code>mark</code> )	$O(1)$	$O(1)$	$O(1)$
Number of calls to <code>get_candidate</code> to get all $k$ ( $k \leq n$ ) unvisited nodes	$k$	$k$	$n$
Required memory in bytes	$4n$	$2n$	$\lceil n/8 \rceil$

implementations is shown in Tab. 1.

#### 4.2. Next node selection

The procedure for the selection of the next node by an ant during the solution construction phase has the biggest impact on the performance of the MMAS and other ACO algorithms [7, 47]. Equation (1) defines the probabilities for selecting each of the unvisited nodes. The sequential version of the procedure has a simple and efficient implementation, often referred to as the *roulette wheel method* (RWM). The RWM takes  $O(n)$  time, where  $n$  is the number of nodes to choose from.

##### 4.2.1. Parallel RWM

The RWM is a typical example of an algorithm that has a simple and efficient sequential implementation but is difficult to parallelize effectively [7]. The difficulties reside in the dependencies between the subsequent computations of the RWM (e.g., the summation of the pheromone and heuristic information products [weights in short]), searching for a "winning" node based on a randomly drawn value. It is not surprising that multiple alternative RWM implementations have been proposed in the literature, including the I-Roulette method by Cecilia et. al [7], the DS-Roulette by Dawson and Stewart [12], and the stochastic trial by Uchida et. al [47]. Although these methods allow for an efficient parallel execution, they are *qualitatively* different from the sequential version [27]. Only recently has Cecilia et. al [8] proposed the parallel *SS-Roulette*

method, which is essentially a parallel version of the RWM, i.e., it offers the same quality of results as the sequential implementation. This was possible mainly due to the increasing computational capacity of GPU architectures, and also improvements on the software side, e.g., the CUDA toolkit.

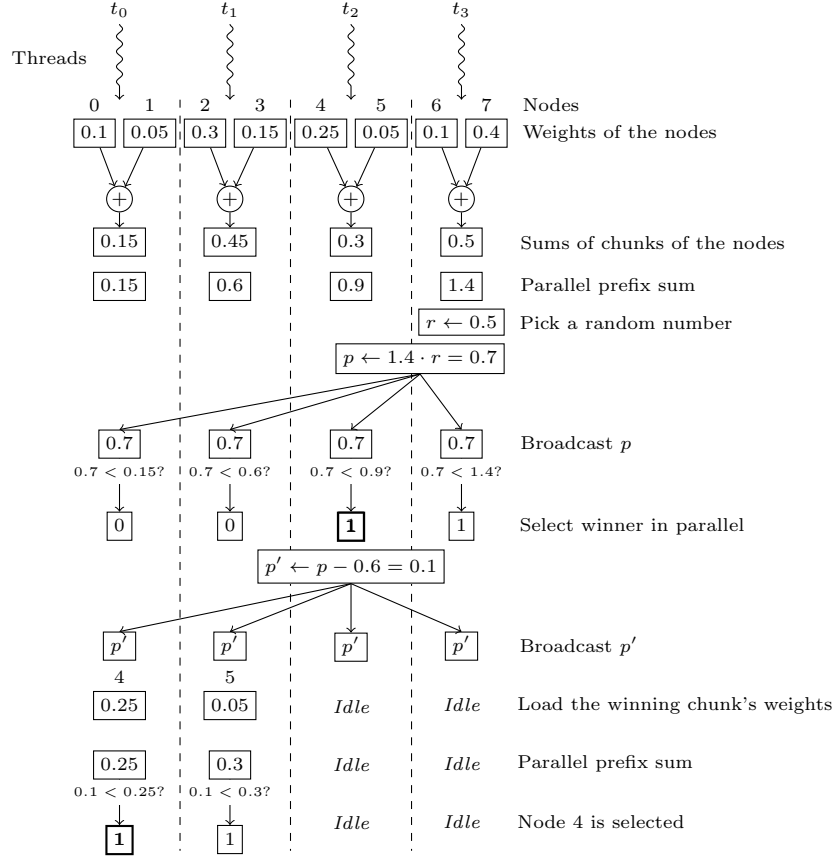


Figure 5: An example showing the execution of the parallel RWM.

Following the description of the SS-Roulette method (as the source code is not available), we have implemented a parallel version of the RWM. Figure 5 shows how our implementation of the parallel RWM (PRWM) works. First, each thread that is executing the PRWM is assigned a chunk of the unvisited nodes, for which it computes a sum of the corresponding weights. Next, a prefix sum of the chunks' sums is computed in parallel. Following this, the last thread draws a uniform random number and multiplies it by the total. The resulting value is broadcast to all threads so that the *winning* chunk of nodes can be selected. If the chunk contains more than one node, then it is necessary to locate the selected node within the chunk. This process again involves the calculation of the prefix sums of the nodes' weights but this time only for the nodes within the chunk. This can also be done in parallel by splitting the chunk's nodes across all threads. In general, this process may require up to  $\lceil \log_p n \rceil$  stages, where  $n$  is the number of nodes and  $p$  is the number of processors. For example, if  $n = 1024$  and  $p = 32$ , then in the first stage each of the 32 threads processes 32-node chunks, and in the second (final) stage each thread is assigned one out of the 32 nodes from the chunk selected during the first stage. It is worth noting that the weights belonging to the chunks selected in a single stage are read from the memory again in the subsequent stage, and so on. Fortunately, the total number of times the weights are read from the memory equals  $\sum_{k=0}^{\lceil \log_p n \rceil} \frac{n}{p^k} \leq n \sum_{k=0}^{\infty} \frac{1}{p^k} = n \frac{p}{p-1}$ , which is  $O(n)$  because the number of threads,  $p$ , is constant.

#### 4.2.2. Weighted Reservoir Sampling

The problem of the selection of the next node in the MMAS can also be seen as an instance of random weighted sampling without replacement, or, more briefly, weighted reservoir sampling (WRS). In WRS, one

has to select  $m$  distinct items randomly out of a population of size  $n$ , while the probability of choosing an item is proportional to its *weight* [17]. In the case of the MMAS, only one item (node) needs to be selected, and the weights are products of the heuristic information values and the pheromone trails values (see Eq. (1)) that are stored in the *choice\_info* matrix.

**Input** : A population  $V$  of  $n$  weighted items  
**Output**: A reservoir (sample)  $R$  with the WRS of size  $m$

- 1 Insert first  $m$  items of  $V$  into  $R$  ;
- 2 **for**  $i \leftarrow 1$  **to**  $m$  **do**
- 3      $k_i \leftarrow u_i^{(1/w_i)}$  where  $u_i = \text{random}(0, 1)$ ;
- 4 **for**  $i \leftarrow m + 1$  **to**  $n$  **do**
- 5      $T \leftarrow$  the smallest key in  $R$  ;
- 6      $k_i \leftarrow u_i^{(1/w_i)}$  where  $u_i = \text{random}(0, 1)$ ;
- 7     **if**  $k_i > T$  **then**
- 8         The item with the minimum key in  $R$  is replaced by item  $v_i$  ;

Figure 6: Algorithm A-Res for computing WRS [17].

Efrimidis and Spirakis proposed an efficient algorithm, named *A-Res* (Fig. 6), for computing WRS [17]. The A-Res algorithm assigns each item a key,  $u_i^{(1/w_i)}$ , where  $u_i$  is a uniformly chosen number from the range  $(0, 1)$ , and then selects  $m$  items with the *largest keys*. The most important property of the algorithm is that it selects the sample in *one pass*, i.e., it considers each item and its weight *once* and, in contrast to the RWM, does not require the summation of all the weights. It also worth noting that the relative order in which the items are processed can be arbitrary, what makes the algorithm easier to parallelize. Therefore, we propose to adapt this algorithm to implement a parallel equivalent of the RWM for application in the MMAS.

- 1  $t \leftarrow \text{threadIdx.x}$  // CUDA-based thread id
- 2  $p \leftarrow \text{blockDim.x}$  // Number of threads in a block
- 3  $R_t \leftarrow \emptyset$  // No element was selected
- 4  $T_t \leftarrow 0$  // Initial key for the thread  $t$
- 5  $l \leftarrow \text{tabu.length}()$
- 6 **for**  $i \leftarrow t$  **to**  $l - 1$  **by**  $p$  **do in parallel** // Thread  $t$  processes indices:  $t, t + p, \dots, \lfloor \frac{n-t}{p} \rfloor p + t$
- 7      $v \leftarrow \text{tabu.get\_candidate}(i)$
- 8     **if**  $v \neq \text{sentinel}$  **then** //  $v$  is an unvisited node
- 9          $r \leftarrow \text{random}(0, 1)$
- 10          $w \leftarrow [\tau_{uv}]^\alpha [\eta_{uv}]^\beta$
- 11          $k \leftarrow r^{(1/w)}$
- 12         **if**  $k > T_t$  **then**
- 13              $T_t \leftarrow k$
- 14              $R_t \leftarrow v$
- 15  $k \leftarrow \arg \max_{i \in \{0, 1, \dots, p-1\}} T_i$  // Parallel reduction of  $(T_0, T_1, \dots, T_{p-1})$
- 16 **return**  $R_k$

Figure 7: The WRS-based parallel pseudo-random proportional selection of the next node in the MMAS.

Figure 7 presents a pseudocode of the parallel version of the WRS (a single thread-block is assumed) adapted to perform the pseudo-random proportional selection of the next node in the MMAS. Each thread starts with its own reservoir that has a size of one (as only one node has to be selected) and the corresponding key (lines 3 and 4). Next, the elements of the tabu are processed by  $p$  threads in parallel (loop in lines 6–14). A thread,  $t$ , processes every  $p$ -th element and selects its own (locally) maximum key,  $T_t$ , and the corresponding element (node)  $R_t$ . After this, a parallel reduction of the keys selected by the threads,  $(T_0, T_1, \dots, T_p)$ , is

performed and the (final) maximum key is elected (line 15). The corresponding element becomes the result of the WRS. The algorithm selects a node in  $O(\frac{L}{p} + \log p)$  time. Figure 8 shows an example of the WRS-based node selection.

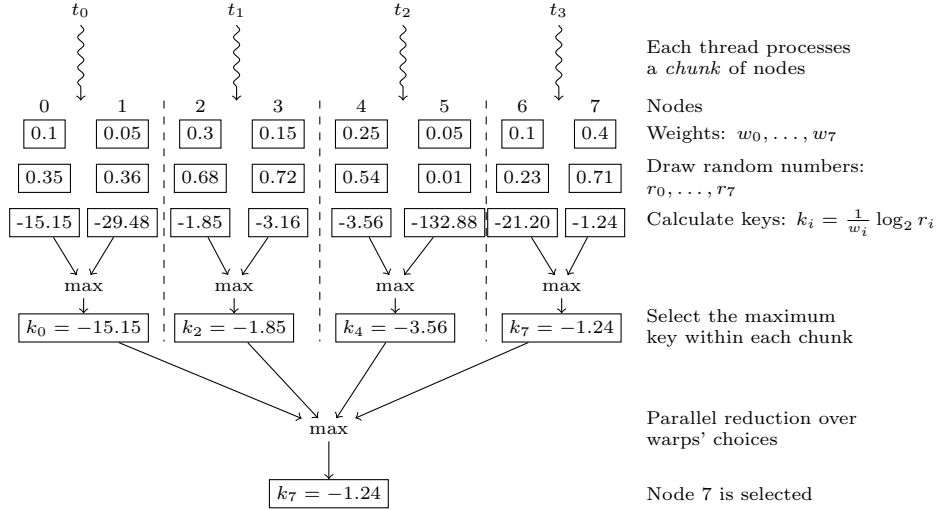


Figure 8: An example showing the execution of the parallel, WRS-based pseudo-random proportional selection of the next node in the MMAS.

The algorithm has a few potential drawbacks that can negatively affect its runtime. Firstly, a single random number is required per element of the tabu, hence a separate pseudo-random number generator's state needs to be stored for each thread. Secondly, the calculation of the keys (line 11 in Fig. 7) involves costly operations on float numbers: division and exponentiation. The former can be alleviated if the reciprocal of each weight (line 10) is calculated in advance. This is possible because the weights depend on the heuristic information values that are constant, while the values of the pheromone trails in the MMAS are updated only once per iteration – after each ant has completed construction of its solution. The latter can be computed using the `powf()` CUDA function but another important problem arises – as the weights are often very small, their reciprocals become large, and therefore so do their exponents. This in turn causes problems, as the 32-bit floating point type does not provide enough precision for the calculations. Fortunately, it is possible to replace the exponentiation with a logarithm, i.e., the calculation in line 11 can be replaced by  $k \leftarrow \frac{1}{w} \log_2 r$ , where  $r$  is a uniform random number in the range  $(0, 1)$  (Also, the initial  $T_t$  value needs to be set carefully as  $\lim_{x \rightarrow 0^+} \log_2 x = -\infty$ ). In fact, it is now possible to use the fast approximate logarithm calculation provided by the CUDA `__log2f()` (intrinsic) function.

#### 4.3. Candidate lists

During the solution construction process an ant located at a given node selects the next node from the set of (yet) unvisited neighboring nodes. If the set of nodes the ant can choose from is limited to the so called *candidate list*, the computation time of the MMAS can be greatly reduced, often without sacrificing quality [43]. The candidate list for each node consists of a number,  $cl$ , of the closest neighboring nodes. Assuming that  $cl$  is constant, the time complexity of the solution construction process for a single ant is reduced from  $O(n^2)$  to  $O(n)$ .

In the original (CPU-based) MMAS implementation for solving the TSP,  $cl = 20$  [43]. Even smaller numbers are possible, however it requires a more complex definition of the *closeness* between nodes, e.g., the  $\alpha$ -measure [19]. In the case of the GPU-based computations, setting  $cl$  to a multiple of the warp size (32 in case of the modern Nvidia GPUs) seems an obvious choice [11].

#### 4.4. Final details

The final structure of the proposed MMAS implementation is shown in Fig. 9. The main component of the parallel MMAS is the ants' solution construction process computed using a single CUDA kernel. We

apply the proven data-parallel approach [7, 11, 47] in which a single thread-block computes the ant’s solution, and the size of each block is a multiple of the warp size, which is 32 in the Nvidia GPUs, so that all the processing elements (CUDA cores) within a warp are used efficiently.

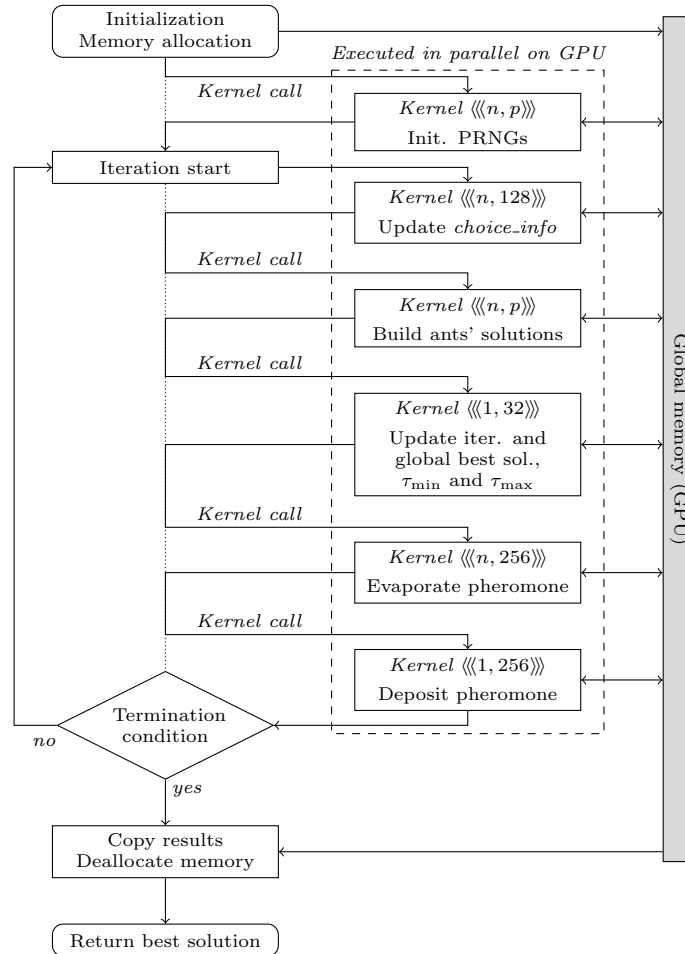


Figure 9: Flowchart of the GPU-based MMAS ( $n$  is the size of the problem,  $p$  is the number of threads per ant). The pairs of numbers in the angle brackets denote the number of thread blocks and the number of threads per block that are executing a kernel, respectively.

After the solutions construction kernel is executed, the iteration best solution is selected. If its cost is lower than the cost of the current global best solution, it becomes the new global best solution and the pheromone trail limits,  $\tau_{\min}$  and  $\tau_{\max}$ , are updated. The new limits are then used by the pheromone evaporation kernel. This kernel is executed with one thread-block per row of the pheromone memory matrix, and with 256 threads in every block. Finally, a pheromone deposition kernel is called. It is responsible for increasing the values of the pheromone trails that correspond to the edges of the iteration best solution. This kernel is executed by a single block of 256 threads.

The presented pheromone evaporation-deposition scheme is simpler than in the AS, in which the pheromone is updated for every ant and where the changes are often conflicting, i.e., they concern the same pheromone trails [7]. In the MMAS, both the evaporation and deposition of the pheromone can be split into *independent* and non-conflicting parts that do not require atomic operations as are used in the GPU-based AS implementations [7, 8].

Table 2: Characteristics of the GPUs used in the computational experiments.

Characteristic	Nvidia Tesla P100	Nvidia Tesla V100
Architecture	Pascal	Volta
Multiprocessors (SM)	56	80
Streaming processors (CUDA cores)	3584	5120
FP32 processing power	9,340 GFLOPS	14,028 GFLOPS
Memory size	16 GB	16 GB
Memory bandwidth	732 GB/s	900 GB/s
L2 cache size (per die)	4,096 KB	6,144 KB
Shared mem. size (per SM)	64 KB	Up to 96 KB
Transistors count	15 Billion	21.1 Billion
Maximum TDP	300W	300W

## 5. Experimental results

In this section we present the results of the computational experiments conducted in order to evaluate the efficiency of the proposed MMAS implementations. The computations were performed on a set of symmetric TSP instances from the well-known TSPLIB [35] repository. The instances were selected so that the results could be compared to the reports available in the literature.

Following the works by Cecilia et. al [7, 8], we set the MMAS parameters as follows:

- the number of ants was equal to the problem size, i.e.,  $m = n$ , where  $n$  denotes the size of the TSP instance;
- $\rho = 0.5$  – the parameter controlling the pheromone evaporation rate;
- $\alpha = 1$  and  $\beta = 2$  – the parameters controlling the influence of the pheromone and the heuristic information on the next node selection probability (Eq. 1);
- the number of iterations equaled 100.

The pheromone trail limits,  $\tau_{\min}$  and  $\tau_{\max}$ , were calculated following the work of Stützle and Hoos [43] with  $p_{\text{best}} = 0.01$ . The initial values of the limits were set based on the value of a solution constructed using the nearest neighbor heuristic. If not stated otherwise, the presented numbers were averaged over 30 repeated executions of a given algorithm. The presented time measurements were obtained using CUDA provided timers and refer to the *kernels* executing respective parts of the MMAS.

Almost all of the computation time in the AS and other ACO algorithms is spent in the solutions construction phase and relatively little on the pheromone updates [7]. This proportion is even higher in the MMAS in which only a single ant deposits pheromone, i.e., the current global or iteration best, depending on the chosen strategy [11]. For this reason, in the computational experiments, we mainly focused on the impact of the tabu and the implementations of the node selection procedure.

Combining the three tabu implementations presented in Section 4.1 and the two node selection procedures in Section 4.2 results in a total of six MMAS variants under consideration. For convenience, they are denoted as MMAS–*node selection procedure*–*tabu implementation*, where the *node selection procedure* is either denoted by RWM or WRS; and *tabu implementation* is denoted by one of the following three: LC, BT and CT tabu implementations.

### 5.1. Computing environment

The implementation of the proposed algorithms was done in C++ using Nvidia CUDA version 10. Sources <sup>1</sup> were compiled using GCC v6.3 with a `-O3` switch for the CPU-side code, while the GPU-side code was compiled with a `-gencode arch=compute_60,code=sm_60` switch for the Nvidia Tesla P100 GPU, and `-gencode arch=compute_70,code=sm_70` switch for the Nvidia Tesla V100 GPU. Table 2 presents the characteristics of the two GPU architectures used. The computations were conducted on servers running under the Debian 9 Linux OS and equipped with a 20-core Intel Xeon 6138 (Skylake) CPU clocked at 2 GHz (a single core was used in the computations).

<sup>1</sup>Sources are available at <https://github.com/RSkinderowicz/GPU-based-MMAS>

## 5.2. Solution construction phase

The efficient use of the computing power offered by GPUs equipped with thousands of processing elements (CUDA cores), requires the proper organization of the computations, i.e., the computations should also be split into multiple, mostly independent portions [26]. In the proposed MMAS implementations we adopted the data-parallel approach in which each ant is assigned a thread-block, and the threads within the thread-blocks are responsible for computing the solution. This leaves one crucial decision: the number of threads within a thread-block. To best adapt to the Nvidia GPUs used in the computations, the size of each thread block was a multiple of the warp size, that is, 32. Although the Volta architecture allows the threads within a warp to follow divergent paths simultaneously [23], setting the number of threads to a multiple of the warp size simplifies the implementation and allows for efficient execution on the pre-Volta generations of GPUs, i.e., Pascal.

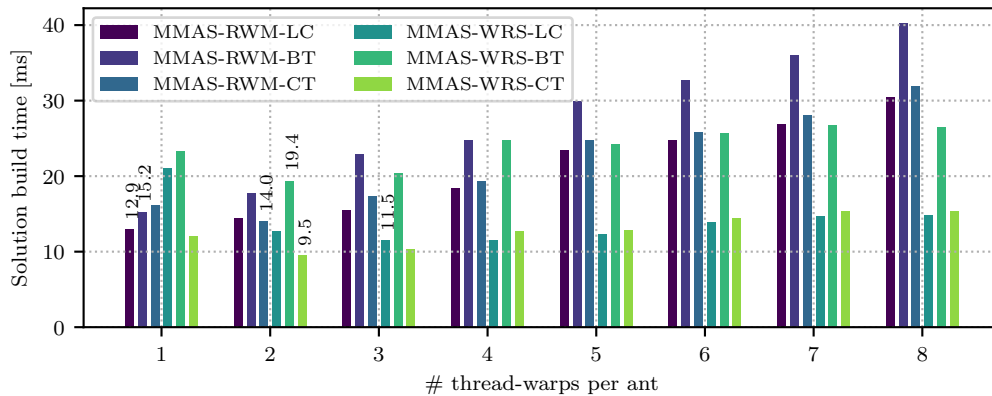


Figure 10: The mean time required by the ants to construct solutions in the MMAS vs. the number of thread-warps per ant for the *pcb1173* instance ( $n$  is the size of the problem). The lowest value for each MMAS variant is shown above the respective bar. The results are for the Nvidia Pascal P100 GPU.

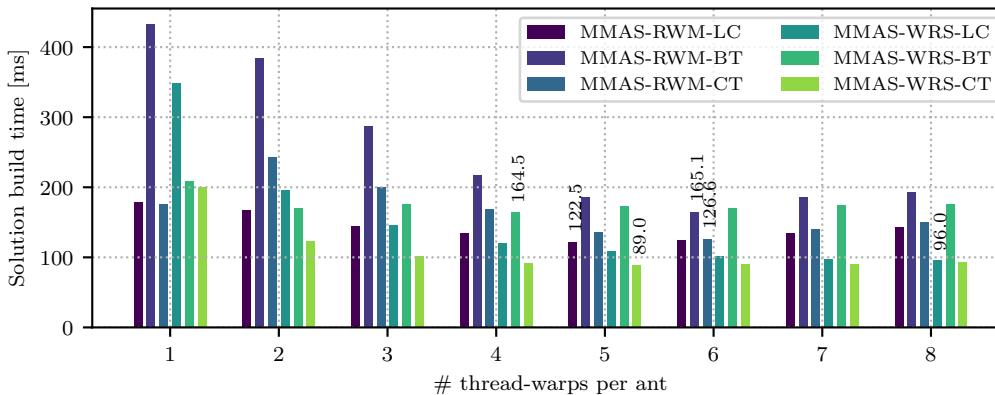


Figure 11: The mean time required by the ants to construct solutions in the MMAS vs. the number of thread-warps per ant for the *pr2392* instance ( $n$  is the size of the problem). The lowest value for each MMAS variant is shown above the respective bar. The results are for the Nvidia P100 GPU.

Figures 10 and 11 show the mean solution construction time for the proposed MMAS variants that executed on the Nvidia P100 GPU vs the number of threads per ant obtained for the *pcb1173* and *pr2392* TSP instances, respectively. A few observations can be made here. First, the MMAS variants differ significantly in speed depending both on the node selection and the tabu implementation. The fastest is the MMAS-WRS-CT variant followed by the MMAS-WRS-LC. The slowest are the variants with the BT, which can be explained by the fact that the BT does not provide direct access to the list of nodes to visit, but checks the status (and the corresponding bit) of each node repeatedly, hence significantly increasing the number of computations.



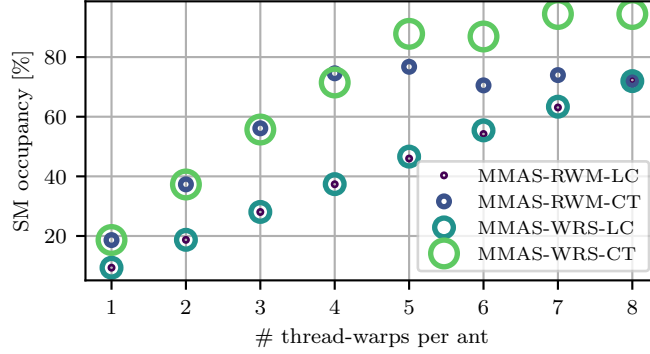


Figure 12: SM occupancy vs. the number of thread warps for the *pr2392* instance and the *Nvidia P100 GPU*.

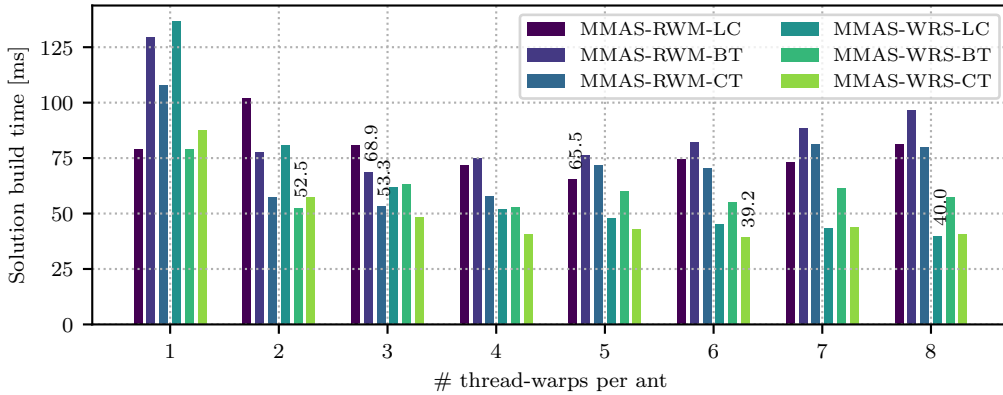


Figure 13: The mean time required for the ants to construct solutions in the MMAS vs. the number of thread-warps per ant for the *pr2392* instance ( $n$  is the size of the problem). The lowest value for each MMAS variant is shown above the respective bar. The results are for the *Nvidia V100 GPU*.

Second, the parallel WRS-based node selection procedure is faster and *scales* better than the parallel RWM implementation. Even though the WRS method involves costly computations (i.e., the random number generation and logarithm calculation), it reduces the number of data exchanges and synchronizations between the threads.

Third, the results indicate that the number of threads should be adjusted to the size of the problem. Specifically, the bigger the problem is, the higher the number of threads per ant are required. This can be observed when comparing the results for the 1,173-city instance (Fig. 10) to the results for the 2,392-city instance (Fig. 11). For the former, the fastest computations were observed for 32 and 64 threads (1 and 2 warps, respectively) per ant; while for the latter, the fastest execution was observed when the number of threads per ant was at least 128 (4 warps). Generally, the efficient use of the GPU's computing power is related to its *occupancy*: understood as the ratio of the number of *active* thread warps to the maximum number of warps per SM [26]. In most cases, this ratio should be high. Often, having more active threads than processing elements (CUDA cores) is beneficial as it allows latencies generated by global memory accesses and synchronization operations to be hidden. The number of thread blocks (each consisting of thread warps) that can execute simultaneously on the same SM is limited by the size of the shared memory and the number of registers used. By increasing the number of ants, we are increasing the number of thread blocks. The LC tabu takes twice as much shared memory as the CT. Thus the latter allows more thread blocks per SM to be executed at the same time. Another, complementary, solution that increases the occupancy is to increase the number of threads per ant. A comparison of occupancy for the proposed MMAS variants with LC and CT tabu implementations solving the *pr2392* TSP instance, is shown in Fig. 12. As can be seen, the CT allows for a higher occupancy, with the MMAS-WRS-CT achieving values exceeding 90% for 7 or 8 thread warps per ant; while for the MMAS with the LC tabu the occupancy does not exceed 80%.

Executing the same MMAS variants on the *Nvidia Volta V100 GPU* reveals a significant advantage in

Table 3: A comparison of the mean solution construction phase times (in ms) for the proposed MMAS variants executed on the *Nvidia P100* GPU. The numbers in parentheses denote the number of thread warps per block (ant). The smallest time for each instance was marked in bold.

Algorithm	Instance							
	<i>d198</i>	<i>pcb442</i>	<i>rat783</i>	<i>pr1002</i>	<i>pcb1173</i>	<i>rl1889</i>	<i>pr2392</i>	<i>fl3795</i>
#1: AS (CPU) [53]	0.87	5.66	25.25	47.17	NA	NA	822.54	NA
#2: AS (GPU) [8]	0.40	1.59	6.81	15.54	23.53	78.87	185.13	726.25
MMAS-RWM-LC	0.33 (1)	1.05 (1)	<b>2.75 (1)</b>	7.77 (1)	12.92 (1)	62.26 (4)	122.46 (5)	482.60 (8)
MMAS-RWM-BT	0.76 (3)	1.37 (1)	3.67 (1)	8.59 (1)	15.25 (1)	83.50 (5)	165.11 (6)	656.51 (10)
MMAS-RWM-CT	0.47 (1)	1.15 (1)	2.80 (1)	6.45 (1)	14.00 (2)	65.05 (4)	126.63 (6)	521.57 (10)
MMAS-WRS-LC	<b>0.30 (2)</b>	<b>0.92 (2)</b>	3.06 (2)	7.68 (3)	11.46 (3)	48.59 (6)	95.96 (8)	383.67 (10)
MMAS-WRS-BT	0.42 (4)	1.58 (2)	6.33 (2)	12.17 (2)	19.37 (2)	94.87 (5)	164.54 (4)	652.62 (6)
MMAS-WRS-CT	0.31 (3)	0.95 (2)	3.18 (2)	<b>6.09 (2)</b>	<b>9.54 (2)</b>	<b>46.02 (5)</b>	<b>88.99 (5)</b>	<b>354.43 (10)</b>
Speedup vs. #1	2.90x	6.14x	9.19x	7.74x	-	-	9.24x	-
Speedup vs. #2	1.33x	1.73x	2.48x	2.55x	2.47x	1.71x	2.08x	2.05x

computing power over the Pascal architecture. This can be seen in Fig. 13, which shows a comparison of the execution times of the solution construction phase for the *pr2392* instance. The fastest variant is again the MMAS-WRS-CT taking about 39.2 ms to complete, vs. 89 ms for the previous generation of GPU. This difference can be somewhat surprising as it cannot be explained simply by the higher processing power, which increased by only about 50%, i.e., 9,340 to 14,028 GFLOP/s. Rather, the advantage can be attributed to a *combination* of multiple factors including an increased number of the processing elements (cores) (see Tab. 2), a larger shared memory per SM, a larger L2 cache, a higher global memory bandwidth and an improved L1 cache replacement policy, among others [23].

Table 3 presents a summary of the mean times needed to execute the MMAS solution construction kernel for the proposed MMAS variants for the Nvidia Tesla P100 GPU. Generally, the MMAS with the WRS-based node selection implementation was faster in all cases but one, while the memory savings resulting from the CT had an impact only for sufficiently large instances, i.e., those with at least 1,000 nodes.

For reference point, we have also provided the results from the two recent works by Zhou et al. [53] and Cecilia et al. [8]. Although in both cases the authors proposed parallel implementations of the AS, the main differences between the AS and the MMAS relate to the pheromone update, while the solution construction phase is analogous, assuming that no candidate lists are used [43]. Specifically, the numbers from Zhou et al. [53] refer to a parallel, multicore-SIMD CPU based AS implementation named VETPAM-CPU-AS, executed on a six-core Intel i7-5820 (Haswell) CPU. The numbers from Cecilia et al. [8] are the execution times of the solution construction kernel for the CUDA-based AS implementation running on an Nvidia GTX TITAN X GPU with 3,072 CUDA cores and 6.69 GFLOP/s of computing power (Maxwell architecture). In comparison, the slower of our GPUs, the Nvidia P100, has about 52% more computing power (single precision), 25% larger L2 cache and more than double the global memory bandwidth (732 GB/s vs. 336 GB/s). The results show that the proposed MMAS-WRS-CT is up to 2.55x faster, which confirms that our implementation utilizes the additional computing resources efficiently. In comparison, the highly optimized VETPAM-CPU-AS is up to 9.24x slower, though still, being very fast if we account for the relatively low computing power of the CPU used for the computations (316 GFLOP/s).

Table 4 shows the results for the Nvidia Volta GPU architecture. In a similar way to the results for the Pascal architecture, the MMASs with the WRS-based implementation were faster than their counterparts with the RWM-based implementation. Specifically, the MMAS-WRS-CT was about 2.88x faster when solving the *pcb1173* instance, but for the larger instances, the speedup dropped to only 2x. This difference can be explained (partially) by the larger L2 cache present in the V100 GPU, 6MB vs. 4MB in the P100 GPU. Storing the *choice\_info* data for the *pcb1173* instance takes up about 5.25MB which fits entirely into the larger cache of the V100 GPU, but only partially into the L2 of the P100 GPU. Generally, the newer GPU offers advantages over the older architecture in all cases, but the differences are larger for medium and large instances, as can be seen in Figure 14.

Compared with the times reported by Cecilia et al. [8], the proposed MMAS implementation is up to 7.18x faster. At the same time, the advantage over the VETPAM-CPU-AS exceeds 20x for the following instances: *rat783*, *pr1002* and *pr2392*.

Table 4: The comparison of duration (in ms) of the mean solution construction phase for the proposed MMAS variants executed on the *Nvidia V100* GPU. The numbers in parentheses denote the number of thread warps per block (ant). The smallest time for each instance is marked in bold.

Algorithm	Instance							
	<i>d198</i>	<i>pcb442</i>	<i>rat783</i>	<i>pr1002</i>	<i>pcb1173</i>	<i>rl1889</i>	<i>pr2392</i>	<i>fl3795</i>
#1: AS (CPU) [53]	0.87	5.66	25.25	47.17	NA	NA	822.54	NA
#2: AS (GPU) [8]	0.40	1.59	6.81	15.54	23.53	78.87	185.13	726.25
MMAS-RWM-LC	0.28 (6)	0.77 (1)	1.87 (1)	3.08 (1)	5.21 (1)	32.75 (4)	65.50 (5)	285.72 (6)
MMAS-RWM-BT	0.42 (1)	1.22 (1)	2.84 (2)	5.04 (2)	7.66 (1)	31.20 (2)	68.90 (3)	301.75 (6)
MMAS-RWM-CT	0.29 (6)	0.81 (1)	1.85 (1)	3.23 (1)	5.55 (1)	24.06 (2)	53.26 (3)	250.62 (6)
MMAS-WRS-LC	<b>0.18 (3)</b>	<b>0.50 (5)</b>	<b>1.26 (4)</b>	<b>2.16 (3)</b>	3.36 (3)	20.39 (5)	40.03 (8)	196.00 (10)
MMAS-WRS-BT	0.23 (4)	0.70 (5)	2.19 (4)	3.85 (4)	5.97 (4)	28.36 (5)	52.54 (2)	236.14 (8)
MMAS-WRS-CT	0.19 (6)	0.52 (5)	1.30 (4)	2.20 (3)	<b>3.31 (3)</b>	<b>19.12 (5)</b>	<b>39.24 (6)</b>	<b>193.05 (10)</b>
Speedup vs. #1	4.77x	11.42x	20.07x	21.79x	-	-	20.96x	-
Speedup vs. #2	2.19x	3.21x	5.41x	7.18x	7.10x	4.12x	4.72x	3.76x

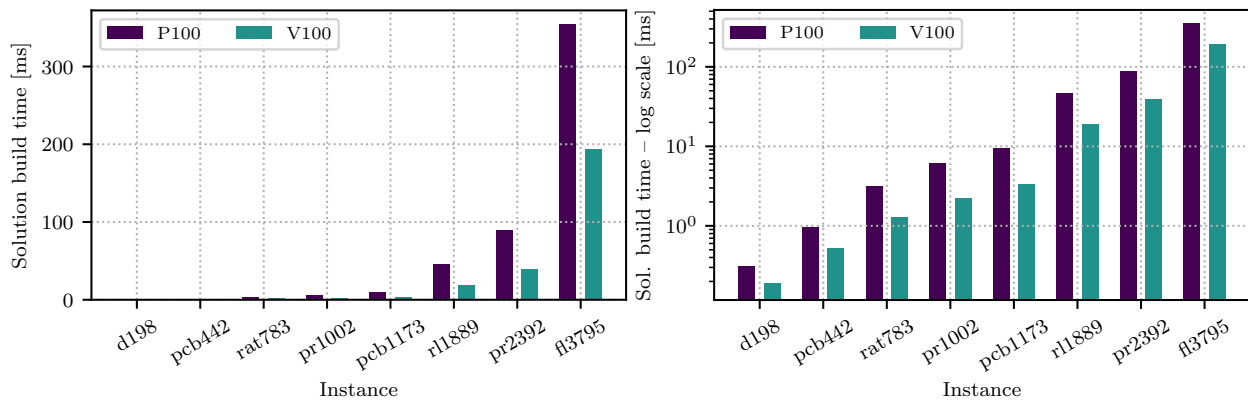


Figure 14: A comparison of the solution construction times for the TSP instances under consideration, obtained for the P100 and V100 GPUs.

Table 5: The mean solution construction phase duration (in ms) for the proposed MMAS variants with a *candidate list* length of 32, executed on the *Nvidia P100 (Pascal)* GPU.

Algorithm	Instance							
	<i>d198</i>	<i>pcb442</i>	<i>rat783</i>	<i>pr1002</i>	<i>pcb1173</i>	<i>rl1889</i>	<i>pr2392</i>	<i>fl3795</i>
AS [11]	0.77	3.67	12.13	19.76	-	-	131.85	-
MMAS-RWM-LC	0.34	0.64	1.11	2.34	2.77	10.09	19.84	88.19
MMAS-RWM-BT	0.35	0.67	1.20	1.70	2.09	<b>6.69</b>	<b>9.33</b>	28.78
MMAS-RWM-CT	0.35	0.67	1.19	1.63	<b>2.01</b>	7.34	12.04	52.32
MMAS-WRS-LC	<b>0.33</b>	<b>0.62</b>	<b>1.09</b>	2.25	2.67	9.70	18.91	85.71
MMAS-WRS-BT	0.34	0.64	1.17	1.69	2.13	6.75	9.44	<b>28.75</b>
MMAS-WRS-CT	0.35	0.65	1.16	<b>1.62</b>	2.07	7.23	11.77	51.08
Speedup vs. AS [11]	2.32x	5.91x	11.18x	12.18x	-	-	14.12x	-

Table 6: The mean solution construction phase duration (in ms) for the proposed MMAS variants with a *candidate list* length of 32, executed on the *Nvidia V100 (Volta)* GPU.

Algorithm	Instance							
	<i>d198</i>	<i>pcb442</i>	<i>rat783</i>	<i>pr1002</i>	<i>pcb1173</i>	<i>rl1889</i>	<i>pr2392</i>	<i>fl3795</i>
AS [11]	0.77	3.67	12.13	19.76	-	-	131.85	-
MMAS-RWM-LC	<b>0.19</b>	0.40	0.72	0.95	1.13	3.54	8.18	32.16
MMAS-RWM-BT	0.20	0.37	0.71	0.97	1.16	2.49	5.18	12.83
MMAS-RWM-CT	0.20	0.41	0.74	1.00	1.20	2.32	5.04	19.32
MMAS-WRS-LC	<b>0.19</b>	0.38	0.69	<b>0.92</b>	<b>1.08</b>	3.40	7.74	30.77
MMAS-WRS-BT	<b>0.19</b>	<b>0.36</b>	<b>0.68</b>	0.93	1.12	2.44	<b>3.26</b>	<b>12.65</b>
MMAS-WRS-CT	<b>0.19</b>	0.40	0.71	0.97	1.15	<b>2.26</b>	4.89	18.66
Speedup vs. AS [11]	4.14x	10.26x	17.84x	21.51x	-	-	40.39x	-

### 5.3. Candidate Lists

Using candidate lists can have a significant impact on the MMAS convergence and also on the execution speed [43]. In our experiments, the length of the candidate lists was set to 32, following Dawson and Stewart [11] who proposed a GPU-based AS using the LC tabu implementation. This value results in a single thread warp per ant. It is worth noting that the V100 GPU has 5,120 CUDA cores, thus we need at least 160 ants to utilize the available computing power. In fact, this number should be even higher to allow for effective memory latency hiding through context switching between the active thread warps [26].

Table 5 presents the mean duration of the solution construction phase for the proposed MMAS implementations. Generally, for the smallest instances, the differences between the algorithms are also small. Only when starting with the *pr1002* instance do the differences increase with performance, mainly depending on the shared memory’s efficiency for the given tabu implementation, with the BT offering the best performance, and the LC the worst (Tab. 1). For example, for the largest instance, *fl3795*, and the MMAS with the WRS node selection implementation; the BT results in a 1.78x and 2.98x speedup over the CT and LC tabu implementations, respectively. The implementation is also up to 14.12x faster than the GPU-based AS by Dawson and Stewart [11] who used the Nvidia GTX 580 GPU (Fermi architecture) with 1,581 GFLOP/s computing power and 192 GB/s global memory bandwidth. As the source code is not available, it is difficult to repeat the computations on the same GPU. However, the observed speedup suggests that our implementation efficiently utilizes the newer GPU’s computing capacity.

Repeating the computations on the newer, Volta V100, GPU results in speedups up to 2.86x for the *pr2392* instance compared to the Pascal P100 GPU. However, for the largest instance, *fl3795*, the speedup falls to 2.27x suggesting that the larger computing capacity of the newer GPU is not able to compensate for the significantly increased number of high-latency memory accesses associated with solving the bigger TSP instance. Compared to the GPU-based AS by Dawson and Stewart [11], the proposed MMAS implementations are up to 40.39x faster. Considering the impact of the node selection procedure and the tabu implementations, the latter is more important, especially for the largest TSP instances.

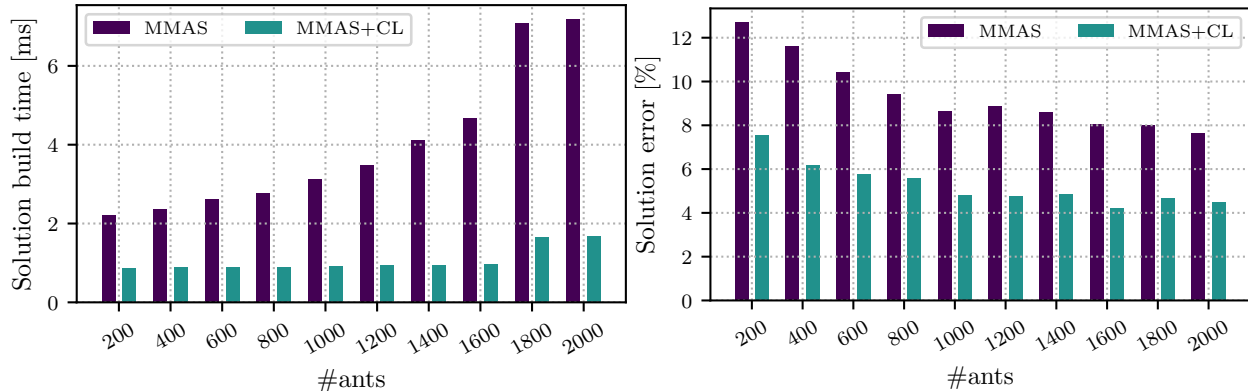


Figure 15: The influence of the number of ants in the MMAS-RWM-CL on the mean solution build time. The results are mean values obtained over 30 runs of the algorithm solving the *pr1002* instance on the Nvidia V100 GPU.

#### 5.4. Varying the number of ants

In the experiments presented above, the number of ants was equal to the size of the instance to enable a comparison with the existing results from the literature [8, 11, 51]. However nothing prevents the number of ants being set to a different value. Figure 15 shows how the number of ants affects the runtime and the quality of the solutions generated by the MMAS-RWM-LC (with and without the CL) solving the *pr1002* instance on the Nvidia V100 GPU. The number of iterations was set to 1,000 and the  $\rho$  parameter governing the pheromone evaporation speed was set to 0.9.

As can be seen, the computation time rises steadily with the increasing number of ants but not as fast as it might be expected based on the numbers alone. This can be explained by the fact that the efficient utilization of the 5,120 computing cores of the Nvidia Tesla V100 GPU (see Tab. 2) requires running a large number of calculations in parallel, i.e., the ants constructing the solutions. On the other hand, each kernel executing on the GPU requires a number of the SM’s registers and a portion of the shared memory to run. Combined with other architecture-related restrictions, the number of thread warps resulting in the best occupancy of the GPU’s SMs can be calculated. For example, the `cudaOccupancyMaxActiveBlocksPerMultiprocessor` function offered by the CUDA framework reports that the best occupancy for the solution construction kernel of the MMAS-RWM-LC (assuming 1 warp per thread block) can be achieved for 1,680 ants. This is consistent with the significant increase in the execution time as observed when going from 1,600 to 1,800 ants.

Focusing on the quality of the solutions, we can observe a positive effect of increasing the number of ants. However, the benefit is much more visible when the number of ants goes from 200 to 1,000, than when it goes from 1,000 to 2,000. In other words, assuming that the number of ants is high enough, it could be more reasonable to increase the number of iterations than to further increase the number of ants.

#### 5.5. Pheromone Update and Remaining Operations

The solution construction process is definitely the most time consuming part of the MMAS. The remaining operations, including the pheromone evaporation and deposition, take significantly less time. Table 7 shows the times needed to complete all the kernels except for the solution construction time for the MMAS-RWM-LC algorithm, as executed on the Pascal and Volta GPUs. The times for the remaining MMAS variants are very close which stems from the fact that most of the differences between the algorithms affect only the solution construction process. As can be seen, the times for the newer-generation Volta GPU are close to two times slower than for the older Pascal GPU. If we compare the numbers to the solution construction kernel times (Tab. 3 and Tab. 4), it can be seen that they are significantly lower and the relative differences increase with the size of the problem. For example, for the *pcb442* instance the solution construction kernel time of the MMAS-WRS-CT executed on the P100 GPU was close to  $7.92x$  greater than the total time needed by all the remaining kernels (0.95 ms vs 0.12 ms). For the largest instance, *fl3795*, the ratio was close to  $246.13x$ , meaning that the solution construction process accounted for over 99.5% of the computation time. The ratio remains high ( $\sim 35.47x$ ) even if the construction process is sped up by using the candidate lists.

Table 7: A comparison of the mean times (in ms) necessary to complete the execution of all kernels except the solution construction for the MMAS-RWM-LC, with a candidate list of 32, executed on the P100 and V100 GPUs.

GPU	Instance							
	<i>d198</i>	<i>pcb442</i>	<i>rat783</i>	<i>pr1002</i>	<i>pcb1173</i>	<i>rl1889</i>	<i>pr2392</i>	<i>f3795</i>
P100 (Pascal)	0.08	0.12	0.21	0.28	0.35	0.61	0.81	1.44
V100 (Volta)	0.05	0.07	0.12	0.15	0.18	0.34	0.44	0.89

Table 8: The results of the non-parametric Friedman test with the null hypothesis  $H_0$  stating that the six proposed MMAS variants produced solutions with the same median quality. The results are provided for each TSP instance separately. Assumed significance level of  $\alpha = 0.05$ .

Instance	<i>d198</i>	<i>pcb442</i>	<i>rat783</i>	<i>pr1002</i>	<i>pcb1173</i>	<i>rl1889</i>	<i>pr2392</i>	<i>f3795</i>
Test statistic	2.13	2.98	3.72	8.76	3.32	6.14	6.41	4.34
<i>p</i> -value	0.83	0.70	0.59	0.12	0.65	0.29	0.27	0.50
$H_0$ rejected	No	No	No	No	No	No	No	No

It is possible that a faster execution of the remaining kernels could be observed if some of them were joined (fused) into one; for example, the pheromone evaporation and deposition kernels. However, as the above analysis has shown, it would have little impact on the overall MMAS execution time while, at the same time, making the implementation more complicated.

### 5.6. Solution Quality

Our work focused on an efficient parallel GPU-based implementation of the MMAS, hence no quality-related modifications of the MMAS were investigated. In fact, to confirm that the proposed MMAS variants differ only in terms of the computation speed, the samples of the final solutions’ quality obtained using the proposed MMAS implementations were checked for statistically significant differences based on the non-parametric Friedman test [20].

The null hypothesis evaluated with this test checks if at least two of the samples represent populations with different median values, in a set of  $k$  samples (where  $k \geq 2$ ). If the null hypothesis is rejected, then the quality of the results generated by the proposed MMAS variants is not equivalent. Table 8 shows the results of the Friedman test for the six proposed MMAS variants: MMAS-RWM-LC, MMAS-RWM-BT, MMAS-RWM-CT, MMAS-WRS-LC, MMAS-WRS-BT and MMAS-WRS-CT. The test was calculated separately for each of the eight TSP instances investigated. As can be seen from Table 8, the null hypothesis was not rejected in any of the cases, hence no statistically significant differences in the quality of the results generated by the MMAS variants were found.

### 5.7. Local Search

The ACO algorithms are typically combined with problem-specific LS heuristics [15]. In this combination, the ACO performs a *coarse-grained* search throughout the space of possible solutions, while the LS is responsible for a fine-grained exploitation of the neighborhood of a solution built by an ant.

For the sake of completeness of the current work, we have implemented a parallel version of the 2-opt heuristic as described by Bentley [4]. The 2-opt works by searching for a pair of edges to remove so that the resulting parts of the route can be reconnected using a new pair of edges that has a combined length smaller than the length of the removed pair. If such an improvement is found and applied, the search is restarted until no further improvements can be found. Although there are only  $O(n^2)$  possible pairs to consider while searching for the improvement, it is still too time-consuming if the number of nodes is on the order of thousands or more. For this reason, in our implementation the performance-oriented heuristics described by Bentley are applied, i.e. the search for a new edge to insert is limited only to the nearest neighbors of the considered node (32 in our case) and an array of so-called *don't look bits* is used to further limit the search. In the proposed parallel version of the 2-opt, a number of threads divided into groups of 32 threads each (warps) search in parallel for the pair of edges to remove, and, if any group succeeds, the improvement is applied (in parallel) by all groups of threads reversing the respective part of the route. The 2-opt is applied to every solution constructed by the ants.

Table 9: A comparison of the results generated by the ESACO [21] and MMAS-RWM-BT (with the 2-opt LS) metaheuristics for the TSP instances from the TSPLIB repository. The best and mean solution costs (route lengths) are given along with the relative difference from the optimum reported in round brackets. The values in the *Time* column refer to the CPU runtime (in seconds) as reported in the respective work and the Nvidia Tesla V100 GPU runtime in the case of the MMAS-RWM-BT. The lowest mean cost for every instance is marked in bold.

Instance	Optimum	ESACO[21]			MMAS-RWM-BT		
		Best solution	Mean solution	Time	Best solution	Mean solution	Time
<i>eil51</i>	426	426 (0%)	<b>426.0 (0%)</b>	1.12	426 (0%)	<b>426.0 (0%)</b>	0.43
<i>eil76</i>	538	538 (0%)	<b>538.0 (0%)</b>	1.39	538 (0%)	<b>538.0 (0%)</b>	0.49
<i>kroA100</i>	21282	21282 (0%)	<b>21282.0 (0%)</b>	2.61	21282 (0%)	<b>21282.0 (0%)</b>	0.58
<i>lin105</i>	14379	14379 (0%)	<b>14379.0 (0%)</b>	2.0	14379 (0%)	<b>14379.0 (0%)</b>	0.6
<i>d198</i>	15780	15780 (0%)	<b>15780.0 (0%)</b>	6.5	15780 (0%)	<b>15780.0 (0%)</b>	0.9
<i>kroA200</i>	29368	29368 (0%)	<b>29368.0 (0%)</b>	4.7	29368 (0%)	<b>29368.0 (0%)</b>	0.8
<i>a280</i>	2579	2579 (0%)	2579.1 (0%)	4.5	2579 (0%)	<b>2579.0 (0%)</b>	1.0
<i>lin318</i>	42029	42029 (0%)	<b>42053.9 (0.06%)</b>	10.2	42029 (0%)	42069.6 (0.1%)	1.7
<i>pcb442</i>	50778	50778 (0%)	<b>50803.6 (0.05%)</b>	11.5	50809 (0.06%)	50950.7 (0.34%)	2.0
<i>att532</i>	27686	27686 (0%)	<b>27701.2 (0%)</b>	23.1	27686 (0%)	27708.9 (0.08%)	1.8
<i>rat783</i>	8806	8806 (0%)	<b>8809.8 (0.04%)</b>	22.6	8810 (0.05%)	8825.5 (0.22%)	3.1
<i>pr1002</i>	259045	259045 (0%)	<b>259509.0 (0.18%)</b>	35.8	259415 (0.14%)	259712.7 (0.26%)	4.0
<i>fl3795</i>	28772	28787 (0.05%)	28883.5 (0.39%)	119.3	28793 (0.07%)	<b>28819.3 (0.16%)</b>	19.5
<i>fnl4461</i>	182566	183254 (0.38%)	<b>183446.0 (0.48%)</b>	192.6	183361 (0.44%)	183627.6 (0.58%)	34.9
<i>rl5915</i>	565530	567177 (0.29%)	568935.0 (0.60%)	216.9	566123 (0.11%)	<b>567699.9 (0.38%)</b>	49.3
<i>pla7397</i>	23260728	23345479 (0.36%)	23389341.0 (0.55%)	213.9	23365046 (0.45%)	<b>23386240.5 (0.54%)</b>	58.0
<i>rl11849</i>	923288	928876 (0.61%)	930338.0 (0.76%)	575.8	926840 (0.38%)	<b>928618.83 (0.58%)</b>	247.4
<i>usa13509</i>	19982859	20172735 (0.95%)	20195089.0 (1.06%)	914.2	20128078 (0.73%)	<b>20168030.2 (0.93%)</b>	224.2
<i>brd14051</i>	469385	473718 (0.92%)	<b>474087.0 (1.00%)</b>	682.5	473389 (0.85%)	474715.65 (1.14%)	228.4
<i>d15112</i>	1573084	1587150 (0.89%)	1589288.0 (1.03%)	776.7	1584054 (0.70%)	<b>1586604.05 (0.86%)</b>	404.2
<i>d18512</i>	645238	652516 (1.13%)	653154.0 (1.23%)	684.4	650784 (0.86%)	<b>651413.58 (0.96%)</b>	335.5

It is worth mentioning, that the GPU-based implementation of the 2-opt was first proposed by Rocki and Suda [38] but without any additional heuristics that could limit the  $O(n^2)$  search space size. The approach was refined by Zhou et al. [52] who improved its execution speed and, combined it with the Iterated Local Search. The authors solved TSP instances of up to 4,461 nodes obtaining for the largest instance solutions with the mean distance from the optimum equal to 3.67%. Another proposal to improve the 2-opt implementation by Rocki and Suda was made by Robinson et al. [37], who allowed multiple non-conflicting changes to a route to be performed simultaneously. The resulting 2-opt hill-climbing with random restarts was used to solve the 7,397-city instance with an error of around 8% relative to the optimum. The GPU-computing power was also utilized to solve the TSP in the work of Wang et al. [49], who proposed a parallel computation model for the self-organizing map neural network. The authors considered instances up to 85,900 cities but the quality of obtained solutions was typically at least 5% above the respective optimum.

To assess the performance of the proposed parallel MMAS with the 2-opt, we conducted a number of experiments using the Nvidia V100 GPU and several instances from the TSPLIB repository with up to 18,512 nodes. Specifically, the MMAS-RWM-BT with the candidate lists of length 32 was run with the number of ants equal to 800 (multiple of the number of 80 SMs in the V100). The values of the remaining parameters were set based on the size of the instance. For the instances with up to  $10^5$  nodes, the number of iterations was 2,000 and the pheromone was evaporated slowly ( $\rho = 0.9$ ), while for the larger instances the number of iterations was increased to 3,000 and the speed of the pheromone evaporation was higher ( $\rho = 0.7$ ). These values were selected with the aim of allowing the algorithm to find good quality solutions within a relatively short time. The computations were repeated 20 times.

Table 9 and Tab. 10 present the obtained results and compare them with the results of two high-performing metaheuristics, namely the Effective Strategies+ACO (ESACO) [21] and the Artificial Bee Colony with a Modified Choice Function (MFC-ABC) [9] (respectively). The ESACO was chosen as it is the current state-of-the-art ACO-based TSP solver. Specifically, it is based on the ACS combined with an efficient LS comprising the 2-opt, 3-opt and so-called *double-bridge moves*. The second algorithm, the MFC-ABC, combines a modified ABC metaheuristic with the well-known Lin-Kernighan heuristic. Extensive comparisons with the existing state-of-the-art metaheuristic TSP solvers showed that the MFC-ABC is very competitive in terms of both computation time and quality of the results [9].

Analysis of the results presented in Tab. 9 and Tab. 10 reveals several facts. Firstly, the proposed MMAS

Table 10: A comparison of the results generated by the MFC-ABC and MMAS-RWM-BT (with the 2-opt LS) metaheuristics. The meaning of the columns is the same as in Tab. 9.

Instance	Optimum	MCF-ABC[9]		MMAS-RWM-BT		
		Mean solution	Time	Best solution	Mean solution	Time
<i>eil101</i>	629	<b>629.0 (0%)</b>	0.0	629 (0%)	<b>629.0 (0%)</b>	0.6
<i>lin105</i>	14379	<b>14379.0 (0%)</b>	0.0	14379 (0%)	<b>14379.0 (0%)</b>	0.6
<i>pr107</i>	44303	<b>44303.0 (0%)</b>	0.0	44303 (0%)	<b>44303.0 (0%)</b>	0.6
<i>gr120</i>	6942	<b>6942.0 (0%)</b>	0.0	6942 (0%)	<b>6942.0 (0%)</b>	0.6
<i>pr124</i>	59030	<b>59030.0 (0%)</b>	0.1	59030 (0%)	<b>59030.0 (0%)</b>	0.6
<i>bier127</i>	118282	<b>118282.0 (0%)</b>	0.1	118282 (0%)	<b>118282.0 (0%)</b>	0.7
<i>ch130</i>	6110	<b>6110.0 (0%)</b>	0.0	6110 (0%)	<b>6110.0 (0%)</b>	0.6
<i>pr136</i>	96772	<b>96772.0 (0%)</b>	0.2	96772 (0%)	<b>96772.0 (0%)</b>	0.6
<i>gr137</i>	69853	<b>69853.0 (0%)</b>	0.1	69853 (0%)	<b>69853.0 (0%)</b>	0.7
<i>pr144</i>	58537	<b>58537.0 (0%)</b>	1.8	58537 (0%)	<b>58537.0 (0%)</b>	0.6
<i>ch150</i>	6528	<b>6528.0 (0%)</b>	0.1	6528 (0%)	<b>6528.0 (0%)</b>	0.7
<i>kroA150</i>	26524	<b>26524.0 (0%)</b>	0.1	26524 (0%)	<b>26524.0 (0%)</b>	0.7
<i>kroB150</i>	26130	<b>26130.0 (0%)</b>	0.1	26130 (0%)	<b>26130.0 (0%)</b>	0.7
<i>pr152</i>	73682	<b>73682.0 (0%)</b>	1.8	73682 (0%)	<b>73682.0 (0%)</b>	0.8
<i>u159</i>	42080	<b>42080.0 (0%)</b>	0.1	42080 (0%)	<b>42080.0 (0%)</b>	0.7
<i>si175</i>	21407	<b>21407.0 (0%)</b>	0.2	21407 (0%)	21407.5 (0%)	0.8
<i>brg180</i>	1950	<b>1950.0 (0%)</b>	0.0	1950 (0%)	<b>1950.0 (0%)</b>	0.7
<i>rat195</i>	2323	<b>2323.0 (0%)</b>	0.2	2323 (0%)	2325.2 (0.2%)	0.8
<i>d198</i>	15780	<b>15780.0 (0%)</b>	1.3	15780 (0%)	<b>15780.0 (0%)</b>	0.9
<i>kroA200</i>	29368	<b>29368.0 (0%)</b>	0.1	29368 (0%)	<b>29368.0 (0%)</b>	0.8
<i>kroB200</i>	29437	<b>29437.0 (0%)</b>	0.0	29437 (0%)	<b>29437.0 (0%)</b>	0.8
<i>gr202</i>	40160	<b>40160.0 (0%)</b>	0.6	40160 (0%)	40161.3 (0%)	0.9
<i>tsp225</i>	3916	<b>3916.0 (0%)</b>	0.0	3916 (0%)	<b>3916.0 (0%)</b>	0.8
<i>ts225</i>	126643	<b>126643.0 (0%)</b>	0.1	126643 (0%)	<b>126643.0 (0%)</b>	0.9
<i>pr226</i>	80369	<b>80369.0 (0%)</b>	1.4	80369 (0%)	<b>80369.0 (0%)</b>	0.9
<i>gr229</i>	134602	<b>134602.0 (0%)</b>	0.8	134602 (0%)	134608.4 (0%)	0.9
<i>gil262</i>	2378	<b>2378.0 (0%)</b>	0.1	2378 (0%)	2378.2 (0.01%)	1.0
<i>pr264</i>	49135	<b>49135.0 (0%)</b>	0.1	49135 (0%)	<b>49135.0 (0%)</b>	1.0
<i>a280</i>	2579	<b>2579.0 (0%)</b>	0.0	2579 (0%)	<b>2579.0 (0%)</b>	1.0
<i>pr299</i>	48191	<b>48191.0 (0%)</b>	0.2	48191 (0%)	48197.1 (0.01%)	1.1
<i>lin318</i>	42029	<b>42029.0 (0%)</b>	1.5	42029 (0%)	42069.6 (0.1%)	1.7
<i>rd400</i>	15281	<b>15281.0 (0%)</b>	2.4	15281 (0%)	15282.9 (0.01%)	1.4
<i>fl417</i>	11861	<b>11861.0 (0%)</b>	5.7	11861 (0%)	<b>11861.0 (0%)</b>	1.6
<i>gr431</i>	171414	<b>171414.0 (0%)</b>	13.0	171414 (0%)	171419.7 (0%)	1.5
<i>pr439</i>	107217	<b>107217.0 (0%)</b>	2.3	107217 (0%)	<b>107217.0 (0%)</b>	1.4
<i>pcb442</i>	50778	<b>50778.0 (0%)</b>	1.6	50809 (0.06%)	50950.7 (0.34%)	2.0
<i>d493</i>	35002	<b>35002.7 (0%)</b>	20.9	35004 (0.01%)	35046.9 (0.13%)	1.7
<i>att532</i>	27686	<b>27686.5 (0%)</b>	11.4	27686 (0%)	27708.9 (0.08%)	1.8
<i>ali535</i>	202339	<b>202339.0 (0%)</b>	10.6	202339 (0%)	202378.1 (0.02%)	2.0
<i>si535</i>	48450	48498.3 (0.1%)	53.3	48450 (0%)	<b>48455.7 (0.01%)</b>	1.9
<i>pa561</i>	2763	<b>2763.1 (0%)</b>	7.1	2763 (0%)	2768.4 (0.20%)	1.8
<i>u574</i>	36905	<b>36905.0 (0%)</b>	2.1	36905 (0%)	36923.2 (0.05%)	2.1
<i>rat575</i>	6773	<b>6774.3 (0.02%)</b>	6.3	6774 (0.01%)	6781.5 (0.13%)	1.9
<i>p654</i>	34643	<b>34643.0 (0%)</b>	21.5	34643 (0%)	34653.6 (0.03%)	2.6
<i>d657</i>	48912	<b>48915.1 (0.01%)</b>	15.5	48913 (0%)	48993.2 (0.17%)	2.3
<i>gr666</i>	294358	<b>294404.8 (0.02%)</b>	32.1	294358 (0%)	294544.3 (0.06%)	2.2
<i>u724</i>	41910	<b>41916.5 (0.02%)</b>	12.9	41929 (0.05%)	41973.8 (0.15%)	2.3
<i>rat783</i>	8806	<b>8806.0 (0%)</b>	4.2	8810 (0.05%)	8825.5 (0.22%)	3.1
<i>dsj1000</i>	18659688	<b>18661580.6 (0.01%)</b>	53.2	18665058 (0.03%)	18677500.3 (0.10%)	4.4
<i>pr1002</i>	259045	<b>259073.0 (0.01%)</b>	16.6	259415 (0.14%)	259712.7 (0.26%)	4.0
<i>si1032</i>	92650	<b>92650.0 (0%)</b>	4.4	92650 (0%)	<b>92650.0 (0%)</b>	3.3
<i>vm1084</i>	239297	<b>239322.3 (0.01%)</b>	24.3	239297 (0%)	239480.0 (0.08%)	3.9
<i>pcb1173</i>	56892	<b>56897.9 (0.01%)</b>	15.4	56892 (0%)	56994.7 (0.18%)	3.8
<i>d1291</i>	50801	<b>50843.7 (0.08%)</b>	15.7	50803 (0%)	50855.5 (0.11%)	4.5
<i>d1655</i>	62128	<b>62221.6 (0.15%)</b>	27.0	62192 (0.10%)	62321.1 (0.31%)	5.7
<i>u1817</i>	57201	<b>57354.2 (0.27%)</b>	24.6	57209 (0.01%)	57428.2 (0.4%)	7.0
<i>u2152</i>	64253	<b>64426.5 (0.27%)</b>	28.3	64366 (0.18%)	64520.1 (0.42%)	7.1
<i>pr2392</i>	378032	<b>378549.6 (0.14%)</b>	28.9	378390 (0.1%)	379872.0 (0.49%)	10.3
<i>fl3795</i>	28772	28825.1 (0.18%)	131.7	28793 (0.07%)	<b>28819.3 (0.16%)</b>	19.5
<i>fnl4461</i>	182566	<b>183002.8 (0.24%)</b>	66.6	183361 (0.44%)	183627.6 (0.58%)	34.9
<i>rl5915</i>	565530	567990.2 (0.44%)	94.2	566123 (0.11%)	<b>567699.9 (0.38%)</b>	49.3
<i>pla7397</i>	23260728	<b>23324321.9 (0.24%)</b>	247.6	23365046 (0.45%)	23386240.5 (0.54%)	58.0
<i>rl11849</i>	923288	<b>928015.1 (0.51%)</b>	308.9	926840 (0.38%)	928618.83 (0.58%)	247.4



with the 2-opt LS is able to obtain good quality results, i.e. within 1% from the optima, for all but one instance, *brd14051*, for which the mean cost was 1.14% above the optimum. As expected, the error increases with the instance size. Secondly, the 2-opt LS is too simplistic to allow the optima to be found except for small instances. On the other hand, it proved to be effective enough to allow the proposed implementation to obtain better results than the ESACO in 14 out of 21 cases, including the largest instances with up to 18,512 cities.

A comparison of the proposed GPU-based MMAS with the MFC-ABC (Tab. 10) confirms the effectiveness of the latter as it generated (on average) better results for 33 out of 63 (52%) instances while worse only for 3. Still, the results obtained for the GPU-based MMAS can be considered satisfactory with the relative error being below 0.5% for all but three (*fnl4461*, *pla7397* and *rl11849*) instances for which it reached 0.58%. Unfortunately, the  $O(n^2)$  memory complexity of the MMAS prevents solving the largest TSP instance (with 85,900 cities) considered in [9] as it would require more than 16 GB of RAM offered by the V100 GPU.

It is also worth adding that the GPU-based MMAS is also competitive in terms of computation time. The average runtime for the instances with less than 10,000 cities was below 1 minute, whereas solving each of the remaining (larger) instances took less than 7 minutes.

Summarizing, the results show that the high computational power of the GPU is enough to allow the relatively simple method (MMAS with the 2-opt) to compete with sophisticated but sequential algorithms. This suggests that more effort should be put into the development of parallel versions of the more advanced LS methods, e.g., the Lin-Kernighan heuristic, allowing the available computing power of multi-core CPUs and the increasingly popular GPUs to be fully utilized.

## 6. Conclusions

The efficient parallel execution of the ACO on GPUs requires a careful organization of the computations, which must harmonize with their capabilities and limitations. A large number of processing elements (cores) allow a high degree of parallelism, and thus require/benefit-from high concurrency. In this paper, we have presented a novel parallel implementation of the solution construction procedure, which is, in general, the most important and the most time-consuming part of the MMAS and ACO. Specifically, we have proposed a novel implementation of the node selection procedure based on the WRS algorithm [17]. It requires little cooperation between parallel threads, resulting in a high degree of scalability, yet it is easy to implement and offers the same quality of generated solutions as does the original RWM-based method. The efficient use of the fast, but size limited, shared memory offered by the SMs that comprise the GPU is also essential from the performance point of view. We have discussed three tabu implementations, namely, LC, CT, and BT, which differ in memory overhead and the time complexity of the offered operations. A total of six MMAS variants have been evaluated empirically on a set of TSP instances ranging from 198 to 3,795 cities. The computations were conducted for two subsequent Nvidia GPU architectures, namely, Pascal (P100) and Volta (V100). In general, the MMAS with the parallel WRS-based node selection implementation is faster than the MMAS with a parallel version of the RWM-based method. The impact of the tabu implementation depends on the size of the problem instance and, more importantly, on the use of the candidate lists. If the candidate lists are used, the BT is preferred as the slow enumerations of its contents are executed rarely. On the other hand, if the lists are not used, then the proposed CT offers better speed at the cost of increased shared memory usage. Overall, the MMAS-WRS-BT and MMAS-WRS-CT are the recommended choices, depending on whether the candidate lists are used or not, respectively. Both GPUs offer excellent performance, with the newer V100 GPU being up to 2.88x faster than the previous-generation P100. For example, the solution construction phase for the *pr1002* instance takes about 6.09 ms on the P100 GPU and only 2.16 on the V100 GPU. If candidate lists with a size of 32 are used, the MMAS-WRS-BT executing on the V100 needs only 0.93 ms, i.e., it generates solutions at the impressive rate of over 1 million solutions per second.

The analysis of the results presented in the literature on speeding up the ACO’s execution using the GPU-based computing shows that huge progress has been made since the emergence of GPUs as a platform for general-purpose computing. For example, it took approximately 392 ms per iteration of the ACO to build solutions to the *pr1002* TSP instance when running on the C2050 (Fermi) GPU [7]. Five GPU generations forward, and the time has decreased to about 2 ms for the V100 (Volta) GPU, that is, 196x faster. Overall, advances in the design of GPU architecture, progress in the development of software tools (compilers, libraries), and algorithmic refinements seem to be a promising answer to the slowing-down of

Moore’s law. Additionally, the computational experiments considering the MMAS combined with the 2-opt LS, show that the high computing speed of GPUs may be sufficient to compete with more sophisticated but sequential algorithms, especially if the results are to be generated quickly.

#### *Future work*

The presented work may be extended in multiple directions. In this paper, we have considered TSP instances for which the tabu fits entirely into the shared (local) memory of a group of threads. However, its size is very limited, up to 64kB or 96kB even for newer Nvidia GPU architectures (Pascal, Volta). If part of the shared memory is reserved for other purposes, for example, a local search procedure, this leaves even less space for the tabu. It may be interesting to consider tabu implementations in which the shared memory is used along with global memory, i.e., variants of the described BT. It is worth adding, that the proposed implementations of the tabu data structure and the WRS-based node selection procedure can be applied to other ACO-based algorithms, for example, the ACS [39], and even to other metaheuristics.

In this present work, we have mostly focused on the algorithmic refinements of the GPU-based ACO implementation, but we think that further improvements are possible. We agree with Cecilia et al. [8] that the new mechanism of cooperative groups introduced in CUDA 9 could prove useful. Also, improvements to the SIMT model introduced in the Volta architecture are worth investigating as they allow for more divergence in the computations performed by the threads belonging to the same warp [32]. Additionally, solving large problem instances would require significant changes to the MMAS to be made, including a replacement of the pheromone memory with a more space-efficient alternative and exploring ideas for alternative, faster proportional selection method implementations.

**Acknowledgments:** This research was supported in part by PL-Grid Infrastructure.

#### References

- [1] CUDA C Programming Guide. URL <https://docs.nvidia.com/cuda/cuda-c-programming-guide/index.html>. [Accessed September 10th, 2018].
- [2] David L. Applegate, Robert E. Bixby, Vasek Chvatal, and William J. Cook. *The Traveling Salesman Problem: A Computational Study (Princeton Series in Applied Mathematics)*. Princeton University Press, Princeton, NJ, USA, 2007. ISBN 0691129932, 9780691129938.
- [3] Hongtao Bai, Dantong OuYang, Ximing Li, Lili He, and Haihong Yu. MAX-MIN ant system on GPU with CUDA. In *Innovative Computing, Information and Control (ICICIC), 2009 Fourth International Conference on*, pages 801–804. IEEE, 2009. DOI: [10.1109/ICICIC.2009.255](https://doi.org/10.1109/ICICIC.2009.255).
- [4] Jon Louis Bentley. Fast algorithms for geometric traveling salesman problems. *INFORMS Journal on Computing*, 4(4): 387–411, 1992. DOI: [10.1287/ijoc.4.4.387](https://doi.org/10.1287/ijoc.4.4.387). URL <https://doi.org/10.1287/ijoc.4.4.387>.
- [5] Andrey Borisenko and Sergei Gorlatch. Comparing gpu-parallelized metaheuristics to branch-and-bound for batch plants optimization. *The Journal of Supercomputing*, pages 1–13, 2018. ISSN 1573-0484. DOI: [10.1007/s11227-018-2472-9](https://doi.org/10.1007/s11227-018-2472-9). URL <https://doi.org/10.1007/s11227-018-2472-9>.
- [6] Alejandro Catalá, Javier Jaén Martínez, and José A. Mocholí. Strategies for accelerating ant colony optimization algorithms on graphical processing units. In *Proceedings of the IEEE Congress on Evolutionary Computation, CEC 2007, 25-28 September 2007, Singapore*, pages 492–500. IEEE, 2007. DOI: [10.1109/CEC.2007.4424511](https://doi.org/10.1109/CEC.2007.4424511). URL <https://doi.org/10.1109/CEC.2007.4424511>.
- [7] José M. Cecilia, José M. García, Andy Nisbet, Martyn Amos, and Manuel Ujaldon. Enhancing data parallelism for ant colony optimization on gpus. *J. Parallel Distrib. Comput.*, 73(1):42–51, 2013. DOI: [10.1016/j.jpdc.2012.01.002](https://doi.org/10.1016/j.jpdc.2012.01.002). URL <https://doi.org/10.1016/j.jpdc.2012.01.002>.
- [8] José M. Cecilia, Antonio Llanes, José L. Abellán, Juan Gómez-Luna, Li-Wen Chang, and Wen-Mei W. Hwu. High-throughput ant colony optimization on graphics processing units. *J. Parallel Distrib. Comput.*, 113:261–274, 2018. DOI: [10.1016/j.jpdc.2017.12.002](https://doi.org/10.1016/j.jpdc.2017.12.002). URL <https://doi.org/10.1016/j.jpdc.2017.12.002>.
- [9] Shin Siang Choong, Li-Pei Wong, and Chee Peng Lim. An artificial bee colony algorithm with a modified choice function for the traveling salesman problem. *Swarm and Evolutionary Computation*, 44:622–635, 2019. DOI: [10.1016/j.swevo.2018.08.004](https://doi.org/10.1016/j.swevo.2018.08.004). URL <https://doi.org/10.1016/j.swevo.2018.08.004>.
- [10] Shu-Chuan Chu, John F. Roddick, and Jeng-Shyang Pan. Ant colony system with communication strategies. *Inf. Sci.*, 167(1-4):63–76, 2004. DOI: [10.1016/j.ins.2003.10.013](https://doi.org/10.1016/j.ins.2003.10.013). URL <https://doi.org/10.1016/j.ins.2003.10.013>.

- [11] Laurence Dawson and Iain A. Stewart. Candidate set parallelization strategies for ant colony optimization on the GPU. In Joanna Kolodziej, Beniamino Di Martino, Domenico Talia, and Kaiqi Xiong, editors, *Algorithms and Architectures for Parallel Processing - 13th International Conference, ICA3PP 2013, Vietri sul Mare, Italy, December 18-20, 2013, Proceedings, Part I*, volume 8285 of *Lecture Notes in Computer Science*, pages 216–225. Springer, 2013. doi: [10.1007/978-3-319-03859-9\\_18](https://doi.org/10.1007/978-3-319-03859-9_18). URL [https://doi.org/10.1007/978-3-319-03859-9\\_18](https://doi.org/10.1007/978-3-319-03859-9_18).
- [12] Laurence Dawson and Iain A. Stewart. Improving ant colony optimization performance on the GPU using CUDA. In *Proceedings of the IEEE Congress on Evolutionary Computation, CEC 2013, Cancun, Mexico, June 20-23, 2013*, pages 1901–1908. IEEE, 2013. doi: [10.1109/CEC.2013.6557791](https://doi.org/10.1109/CEC.2013.6557791). URL <https://doi.org/10.1109/CEC.2013.6557791>.
- [13] Jérémy Decerle, Olivier Grunder, Amir Hajjam El Hassani, and Oussama Barakat. A hybrid memetic-ant colony optimization algorithm for the home health care problem with time window, synchronization and working time balancing. *Swarm and Evolutionary Computation*, 46:171–183, 2019. doi: [10.1016/j.swevo.2019.02.009](https://doi.org/10.1016/j.swevo.2019.02.009). URL <https://doi.org/10.1016/j.swevo.2019.02.009>.
- [14] Audrey Delévacq, Pierre Delisle, Marc Gravel, and Michaël Krajecki. Parallel ant colony optimization on graphics processing units. *J. Parallel Distrib. Comput.*, 73(1):52–61, 2013. doi: [10.1016/j.jpdc.2012.01.003](https://doi.org/10.1016/j.jpdc.2012.01.003). URL <https://doi.org/10.1016/j.jpdc.2012.01.003>.
- [15] Marco Dorigo and Thomas Stützle. *Ant colony optimization*. MIT Press, 2004. ISBN 978-0-262-04219-2. doi: [10.7551/mitpress/1290.001.0001](https://doi.org/10.7551/mitpress/1290.001.0001). URL <https://doi.org/10.7551/mitpress/1290.001.0001>.
- [16] Marco Dorigo, Vittorio Maniezzo, and Alberto Coloni. Ant system: optimization by a colony of cooperating agents. *IEEE Trans. Systems, Man, and Cybernetics, Part B*, 26(1):29–41, 1996. doi: [10.1109/3477.484436](https://doi.org/10.1109/3477.484436). URL <https://doi.org/10.1109/3477.484436>.
- [17] Pavlos S. Efrimidis and Paul G. Spirakis. Weighted random sampling with a reservoir. *Inf. Process. Lett.*, 97(5):181–185, 2006. doi: [10.1016/j.ipl.2005.11.003](https://doi.org/10.1016/j.ipl.2005.11.003). URL <https://doi.org/10.1016/j.ipl.2005.11.003>.
- [18] Andries Petrus Engelbrecht. *Fundamentals of Computational Swarm Intelligence*. Wiley, 2005. ISBN 978-0-470-09191-3. URL <http://eu.wiley.com/WileyCDA/WileyTitle/productCd-0470091916.html>.
- [19] Keld Helsgaun. General  $k$ -opt submoves for the lin-kernighan TSP heuristic. *Math. Program. Comput.*, 1(2-3):119–163, 2009. doi: [10.1007/s12532-009-0004-6](https://doi.org/10.1007/s12532-009-0004-6). URL <https://doi.org/10.1007/s12532-009-0004-6>.
- [20] Myles Hollander, Douglas A Wolfe, and Eric Chicken. *Nonparametric statistical methods, Third Edition*. John Wiley & Sons, 2015. ISBN 978-0-47-038737-5. doi: [10.1002/9781119196037](https://doi.org/10.1002/9781119196037).
- [21] Hassan Ismikhani. Effective heuristics for ant colony optimization to handle large-scale problems. *Swarm and Evolutionary Computation*, 32:140–149, 2017. doi: [10.1016/j.swevo.2016.06.006](https://doi.org/10.1016/j.swevo.2016.06.006). URL <https://doi.org/10.1016/j.swevo.2016.06.006>.
- [22] Zhao-Hong Jia, Xue-Xue Zhuo, Joseph Y.-T. Leung, and Kai Li. Integrated production and transportation on parallel batch machines to minimize total weighted delivery time. *Computers & OR*, 102:39–51, 2019. doi: [10.1016/j.cor.2018.07.026](https://doi.org/10.1016/j.cor.2018.07.026). URL <https://doi.org/10.1016/j.cor.2018.07.026>.
- [23] Zhe Jia, Marco Maggioni, Benjamin Staiger, and Daniele Paolo Scarpazza. Dissecting the NVIDIA volta GPU architecture via microbenchmarking. *CoRR*, abs/1804.06826, 2018. URL <http://arxiv.org/abs/1804.06826>.
- [24] Raka Jovanovic, Milan Tuba, and Stefan Voß. An efficient ant colony optimization algorithm for the blocks relocation problem. *European Journal of Operational Research*, 274(1):78–90, 2019. doi: [10.1016/j.ejor.2018.09.038](https://doi.org/10.1016/j.ejor.2018.09.038). URL <https://doi.org/10.1016/j.ejor.2018.09.038>.
- [25] James Kennedy. Swarm intelligence. In Albert Y. Zomaya, editor, *Handbook of Nature-Inspired and Innovative Computing - Integrating Classical Models with Emerging Technologies*, pages 187–219. Springer, 2006. doi: [10.1007/0-387-27705-6\\_6](https://doi.org/10.1007/0-387-27705-6_6). URL [https://doi.org/10.1007/0-387-27705-6\\_6](https://doi.org/10.1007/0-387-27705-6_6).
- [26] David Blair Kirk and Wen-mei W. Hwu. *Programming Massively Parallel Processors - A Hands-on Approach*. Morgan Kaufmann, 2010. ISBN 978-0-12-381472-2. URL [http://www.elsevier.com/wps/find/bookdescription.cws\\_home/722320/description#description](http://www.elsevier.com/wps/find/bookdescription.cws_home/722320/description#description).
- [27] Huw Lloyd and Martyn Amos. Analysis of independent roulette selection in parallel ant colony optimization. In Peter A. N. Bosman, editor, *Proceedings of the Genetic and Evolutionary Computation Conference, GECCO 2017, Berlin, Germany, July 15-19, 2017*, pages 19–26. ACM, 2017. doi: [10.1145/3071178.3071308](https://doi.org/10.1145/3071178.3071308). URL <https://doi.org/10.1145/3071178.3071308>.
- [28] Manuel López-Ibáñez, Thomas Stützle, and Marco Dorigo. Ant colony optimization: A component-wise overview. In Rafael Martí, Panos M. Pardalos, and Mauricio G. C. Resende, editors, *Handbook of Heuristics*, pages 371–407. Springer, 2018. doi: [10.1007/978-3-319-07124-4\\_21](https://doi.org/10.1007/978-3-319-07124-4_21). URL [https://doi.org/10.1007/978-3-319-07124-4\\_21](https://doi.org/10.1007/978-3-319-07124-4_21).

- [29] Guo-Heng Luo, Sheng-Kai Huang, Yue-Shan Chang, and Shyan-Ming Yuan. A parallel bees algorithm implementation on GPU. *Journal of Systems Architecture - Embedded Systems Design*, 60(3):271–279, 2014. doi: [10.1016/j.sysarc.2013.09.007](https://doi.org/10.1016/j.sysarc.2013.09.007). URL <https://doi.org/10.1016/j.sysarc.2013.09.007>.
- [30] Max Manfrin, Mauro Birattari, Thomas Stützle, and Marco Dorigo. Parallel ant colony optimization for the traveling salesman problem. In Marco Dorigo, Luca Maria Gambardella, Mauro Birattari, Alcherio Martinoli, Riccardo Poli, and Thomas Stützle, editors, *Ant Colony Optimization and Swarm Intelligence, 5th International Workshop, ANTS 2006, Brussels, Belgium, September 4-7, 2006, Proceedings*, volume 4150 of *Lecture Notes in Computer Science*, pages 224–234. Springer, 2006. doi: [10.1007/11839088\\_20](https://doi.org/10.1007/11839088_20). URL [https://doi.org/10.1007/11839088\\_20](https://doi.org/10.1007/11839088_20).
- [31] Luca Mussi, Fabio Daolio, and Stefano Cagnoni. Evaluation of parallel particle swarm optimization algorithms within the cuda™ architecture. *Information Sciences*, 181(20):4642–4657, 2011.
- [32] NVIDIA Corporation. NVIDIA Tesla V100 GPU Architecture, 2017. URL <http://images.nvidia.com/content/volta-architecture/pdf/volta-architecture-whitepaper.pdf>.
- [33] Martín Pedemonte, Sergio Nesmachnow, and Héctor Cancela. A survey on parallel ant colony optimization. *Appl. Soft Comput.*, 11(8):5181–5197, 2011. doi: [10.1016/j.asoc.2011.05.042](https://doi.org/10.1016/j.asoc.2011.05.042). URL <https://doi.org/10.1016/j.asoc.2011.05.042>.
- [34] Marcus Randall and Andrew Lewis. A parallel implementation of ant colony optimization. *J. Parallel Distrib. Comput.*, 62(9):1421–1432, 2002. doi: [10.1006/jpdc.2002.1854](https://doi.org/10.1006/jpdc.2002.1854). URL <https://doi.org/10.1006/jpdc.2002.1854>.
- [35] Gerhard Reinelt. TSPLIB - A traveling salesman problem library. *INFORMS Journal on Computing*, 3(4):376–384, 1991. doi: [10.1287/ijoc.3.4.376](https://doi.org/10.1287/ijoc.3.4.376). URL <https://doi.org/10.1287/ijoc.3.4.376>.
- [36] Anton Rey, Manuel Prieto, José Ignacio Gómez, Christian Tenllado, and José Ignacio Hidalgo. A CPU-GPU parallel ant colony optimization solver for the vehicle routing problem. In Kevin Sim and Paul Kaufmann, editors, *Applications of Evolutionary Computation - 21st International Conference, EvoApplications 2018, Parma, Italy, April 4-6, 2018, Proceedings*, volume 10784 of *Lecture Notes in Computer Science*, pages 653–667. Springer, 2018. doi: [10.1007/978-3-319-77538-8\\_44](https://doi.org/10.1007/978-3-319-77538-8_44). URL [https://doi.org/10.1007/978-3-319-77538-8\\_44](https://doi.org/10.1007/978-3-319-77538-8_44).
- [37] Jeffrey A. Robinson, Susan V. Vrbsky, Xiaoyan Hong, and Brian P. Eddy. Analysis of a high-performance TSP solver on the GPU. *ACM Journal of Experimental Algorithmics*, 23, 2018. doi: [10.1145/3154835](https://doi.org/10.1145/3154835). URL <https://doi.org/10.1145/3154835>.
- [38] Kamil Rocki and Reiji Suda. High performance GPU accelerated local optimization in TSP. In *2013 IEEE International Symposium on Parallel & Distributed Processing, Workshops and Phd Forum, Cambridge, MA, USA, May 20-24, 2013*, pages 1788–1796. IEEE, 2013. doi: [10.1109/IPDPSW.2013.227](https://doi.org/10.1109/IPDPSW.2013.227). URL <https://doi.org/10.1109/IPDPSW.2013.227>.
- [39] Rafał Skinderowicz. The GPU-based parallel Ant Colony System. *J. Parallel Distrib. Comput.*, 98:48–60, 2016. doi: [10.1016/j.jpdc.2016.04.014](https://doi.org/10.1016/j.jpdc.2016.04.014). URL <https://doi.org/10.1016/j.jpdc.2016.04.014>.
- [40] Rafał Skinderowicz. An improved ant colony system for the sequential ordering problem. *Computers & OR*, 86:1–17, 2017. doi: [10.1016/j.cor.2017.04.012](https://doi.org/10.1016/j.cor.2017.04.012). URL <https://doi.org/10.1016/j.cor.2017.04.012>.
- [41] Rafał Skinderowicz. Solving the uncapacitated traveling purchaser problem with the MAX-MIN ant system. In Ngoc Thanh Nguyen, Elias Pimenidis, Zaheer Khan, and Bogdan Trawiński, editors, *Computational Collective Intelligence - 10th International Conference, ICCCI 2018, Bristol, UK, September 5-7, 2018. Proceedings, Part II*, volume 11056 of *Lecture Notes in Computer Science*, pages 257–267. Springer, 2018. doi: [10.1007/978-3-319-98446-9\\_24](https://doi.org/10.1007/978-3-319-98446-9_24). URL [https://doi.org/10.1007/978-3-319-98446-9\\_24](https://doi.org/10.1007/978-3-319-98446-9_24).
- [42] Erich Strohmaier, Jack Dongarra, Horst Simon, and Martin Meuer. TOP500 Supercomputer Site. URL <http://top500.org>. [Accessed November 21st, 2018].
- [43] Thomas Stützle and Holger H. Hoos. MAX-MIN ant system. *Future Generation Comp. Syst.*, 16(8):889–914, 2000. doi: [10.1016/S0167-739X\(00\)00043-1](https://doi.org/10.1016/S0167-739X(00)00043-1). URL [https://doi.org/10.1016/S0167-739X\(00\)00043-1](https://doi.org/10.1016/S0167-739X(00)00043-1).
- [44] El-Ghazali Talbi, Olivier Roux, Cyril Fonlupt, and D. Robillard. Parallel ant colonies for the quadratic assignment problem. *Future Generation Comp. Syst.*, 17(4):441–449, 2001. doi: [10.1016/S0167-739X\(99\)00124-7](https://doi.org/10.1016/S0167-739X(99)00124-7). URL [https://doi.org/10.1016/S0167-739X\(99\)00124-7](https://doi.org/10.1016/S0167-739X(99)00124-7).
- [45] Ying Tan and Ke Ding. A survey on gpu-based implementation of swarm intelligence algorithms. *IEEE Trans. Cybernetics*, 46(9):2028–2041, 2016. doi: [10.1109/TCYB.2015.2460261](https://doi.org/10.1109/TCYB.2015.2460261). URL <https://doi.org/10.1109/TCYB.2015.2460261>.
- [46] Neil Thompson and Svenja Spanuth. The decline of computers as a general purpose technology: Why deep learning and the end of moore’s law are fragmenting computing. *Available at SSRN 3287769*, 2018. URL <http://dx.doi.org/10.2139/ssrn.3287769>.

- [47] Akihiro Uchida, Yasuaki Ito, and Koji Nakano. An efficient GPU implementation of ant colony optimization for the traveling salesman problem. In *Third International Conference on Networking and Computing, ICNC 2012, Okinawa, Japan, December 5-7, 2012*, pages 94–102. IEEE Computer Society, 2012. doi: [10.1109/ICNC.2012.22](https://doi.org/10.1109/ICNC.2012.22). URL <https://doi.org/10.1109/ICNC.2012.22>.
- [48] Olgierd Unold and Radoslaw Tarnawski. A parallel framework for multi-population cultural algorithm and its applications in TSP. In Giuseppe Nicosia, Panos M. Pardalos, Giovanni Giuffrida, and Renato Umeton, editors, *Machine Learning, Optimization, and Big Data - Third International Conference, MOD 2017, Volterra, Italy, September 14-17, 2017, Revised Selected Papers*, volume 10710 of *Lecture Notes in Computer Science*, pages 470–482. Springer, 2017. doi: [10.1007/978-3-319-72926-8\\_39](https://doi.org/10.1007/978-3-319-72926-8_39). URL [https://doi.org/10.1007/978-3-319-72926-8\\_39](https://doi.org/10.1007/978-3-319-72926-8_39).
- [49] Hongjian Wang, Naiyu Zhang, and Jean-Charles Créput. A massively parallel neural network approach to large-scale euclidean traveling salesman problems. *Neurocomputing*, 240:137–151, 2017. doi: [10.1016/j.neucom.2017.02.041](https://doi.org/10.1016/j.neucom.2017.02.041). URL <https://doi.org/10.1016/j.neucom.2017.02.041>.
- [50] Jiening Wang, Jiankang Dong, and Chunfeng Zhang. Implementation of Ant Colony Algorithm Based on GPU. In Ebad Banissi, Muhammad Sarfraz, Jiawan Zhang, Anna Ursyn, Wong Chow Jeng, Mark W. McK. Bannatyne, Jian J. Zhang, Lim Hwee San, and Mao Lin Huang, editors, *Sixth International Conference on Computer Graphics, Imaging and Visualization: New Advances and Trends, CGIV 2009, 11-14 August 2009, Tianjin, China*, pages 50–53. IEEE Computer Society, 2009. doi: [10.1109/CGIV.2009.20](https://doi.org/10.1109/CGIV.2009.20). URL <https://doi.org/10.1109/CGIV.2009.20>.
- [51] Wei Zhou, Fazhi He, and Zhengchang Zhang. A GPU-based parallel MAX-MIN Ant System algorithm with grouped roulette wheel selection. In Weiming Shen, Pedro Antunes, Nguyen Hoang Thuan, Jean-Paul A. Barthès, Junzhou Luo, and Jianming Yong, editors, *21st IEEE International Conference on Computer Supported Cooperative Work in Design, CSCWD 2017, Wellington, New Zealand, April 26-28, 2017*, pages 360–365. IEEE, 2017. ISBN 978-1-5090-6199-0. doi: [10.1109/CSCWD.2017.8066721](https://doi.org/10.1109/CSCWD.2017.8066721). URL <https://doi.org/10.1109/CSCWD.2017.8066721>.
- [52] Yi Zhou, Fazhi He, and Yimin Qiu. Optimization of parallel iterated local search algorithms on graphics processing unit. *The Journal of Supercomputing*, 72(6):2394–2416, 2016. doi: [10.1007/s11227-016-1738-3](https://doi.org/10.1007/s11227-016-1738-3). URL <https://doi.org/10.1007/s11227-016-1738-3>.
- [53] Yi Zhou, Fazhi He, Neng Hou, and Yimin Qiu. Parallel ant colony optimization on multi-core SIMD cpus. *Future Generation Comp. Syst.*, 79:473–487, 2018. doi: [10.1016/j.future.2017.09.073](https://doi.org/10.1016/j.future.2017.09.073). URL <https://doi.org/10.1016/j.future.2017.09.073>.